

Chapter 2

CTMQC applied to the Tully Models

The Tully models, first proposed by John Tully in 1990⁸¹, are a collection of simple ~~4~~one dimensional model systems. They were designed to be simple enough to obtain accurate quantum results to benchmark new nonadiabatic molecular dynamics (NAMD) methods against. Originally there were ~~3,1~~ three, one dimensional, ~~4~~single atom models. However, in this work an extra model has been introduced with parameters taken from Gossel³. This is to allow a full comparison of my implementation of CTMQC with the literature. In this chapter my implementation of CTMQC will be tested using these model systems and by comparing my results with those in the literature.

In each of the Tully models the (diabatic) Hamiltonian is a function of nuclear positions , \mathbf{R} and is a 2×2 matrix that takes the form:

$$\hat{H} = \frac{\hat{P}^2}{2M} + \begin{pmatrix} H_{11}(\mathbf{R}) & H_{12}(\mathbf{R}) \\ H_{21}(\mathbf{R}) & H_{22}(\mathbf{R}) \end{pmatrix} \quad (2.1)$$

The nuclear mass has been set to 2000 a.u.. This was set to be very close to the proton's mass of 1836 a.u. so we can expect significant quantum effects that classical theory couldn't replicate. The values of the Hamiltonian matrix elements are set to produce systems that resemble common features in a typical nonadiabatic simulation such as avoided crossings and regions of extended coupling. The parameters used in each systems' Hamiltonian where taken from Gossel³ in order to compare the 2 implementations. These can be found in appendix A.

In order to propagate dynamics in the adiabatic basis we need to calculate various quantities from the hamiltonian at each timestep. These are, for Ehrenfest, the (adiabatic) nonadiabatic coupling vector ($\mathbf{d}_{lk}^{(I)}$) and the adiabatic energies ($E_l^{(I)}$). In the full CTMQC simulations we must also calculate the adiabatic momentum term $\mathbf{f}_l^{(I)}$ from the Hamiltonian. The adiabatic energies are the eigenvalues of the Hamiltonian. The adiabatic NACV can be calculated via a finite difference method and equation (2.2) below.

$$\mathbf{d}_{lk}^{(I)} = \langle \psi_l^{(I)} | \nabla \psi_k^{(I)} \rangle \quad (2.2)$$

Where $\psi_l^{(I)}$ is the adiabatic electronic basis function for adiabatic state l . This is given by the eigenvector of the Hamiltonian, on replica I , corresponding to state l . Illustrations of these two properties can be found below in fig 2.1 for each of the four model systems.

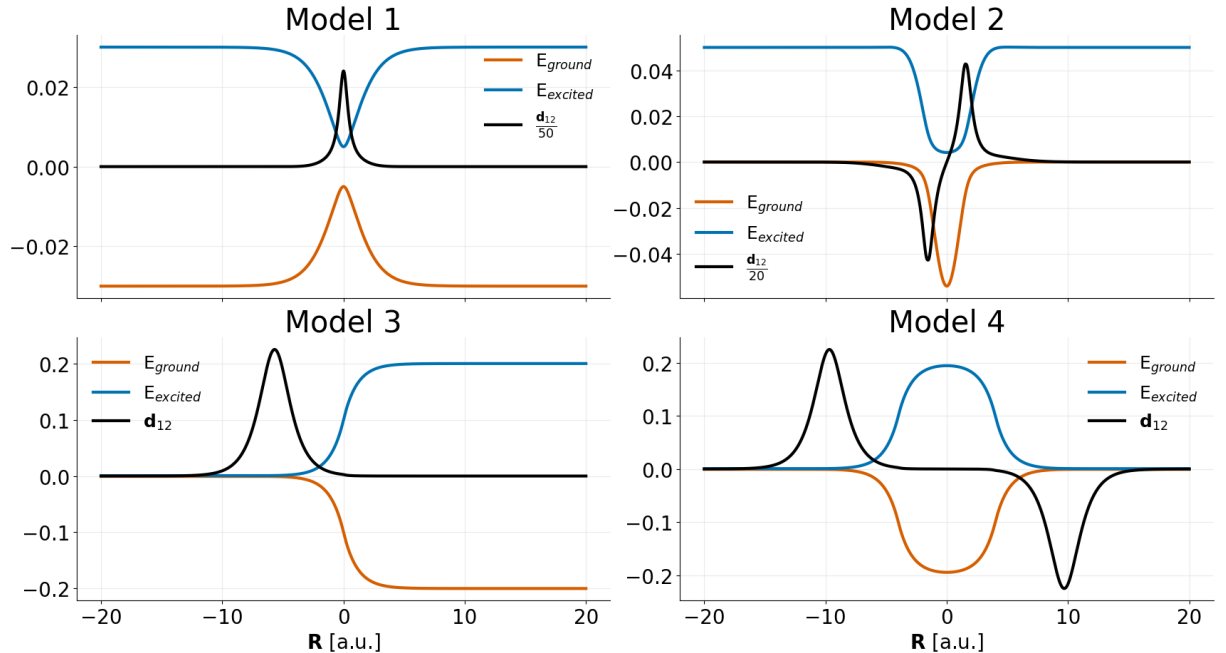


Figure 2.1: Adiabatic potential energy surfaces (orange and blue) and element 1, 2 of the nonadiabatic coupling vector (black) for the four model systems. For parameters see appendix A.

In order to initialise the simulations coordinates and velocities were sampled from the Wigner phase-space distribution of a gaussian nuclear wavepackets given by equation (2.3). A derivation of this can be found in appendix B. The nuclear positions/velocities were then propagated using a velocity verlet algorithm and the adiabatic expansion coefficients were propagated using a 4th order Runge-Kutta method.

$$\chi(R, 0) = \frac{1}{(\pi\mu^2)^{\frac{1}{4}}} e^{-\frac{(R-R_0)^2}{2\mu^2} + ik_0(R-R_0)} \quad (2.3)$$

The adiabatic coefficients were initialised purely on the ground state and the initial width of the nuclear wavepacket was set to $\mu = \sqrt{2}$ bohr. This was chosen to replicate values found in the literature³. Two values of initial momenta k_0 were chosen for each model, one low value and another higher one. Full details of all input parameters can be found in appendix A. I have implemented a serial version of CTMQC acting on Tully's toy model systems and real molecular systems using couplings derived from the analytic overlap method⁶¹ within the software package CP2K⁸² and for Tully's model systems as standalone python code. These are accessible publicly via github repositories at: github.com/95ellismle. This work will only focus on results from the CP2K implementation as we will later see this code extended and applied to systems of real Ethylene molecules.

2.1 Testing My Implementation -Ehrenfest

The motivation behind implementing CTMQC for the Tully models was to serve as a verifiable base for later extensions, such as integrating CTMQC within the fragment-orbital based (FOB)⁸³ framework which will be discussed in a later chapter 4.4. Using such simple systems will also help to clarify how each new parameter works and make testing and debugging easier. As well as many numerical tests on individual terms in the equations, I have implemented some physical tests on the overall system dynamics. In this section, I will outline the key tests I have performed on the Ehrenfest propagation and will include the full details of the full CTMQC propagation in the following section.

In all the simulations when the Tully models are referenced they will refer to those

parameters given in appendix A. Reference to a high momentum Tully model simulation is a reference to that model with initial momenta being sampled from the Wigner distribution of the higher of the ~~2~~^{two} initial momenta given in appendix A.

2.1.1 Norm Conservation

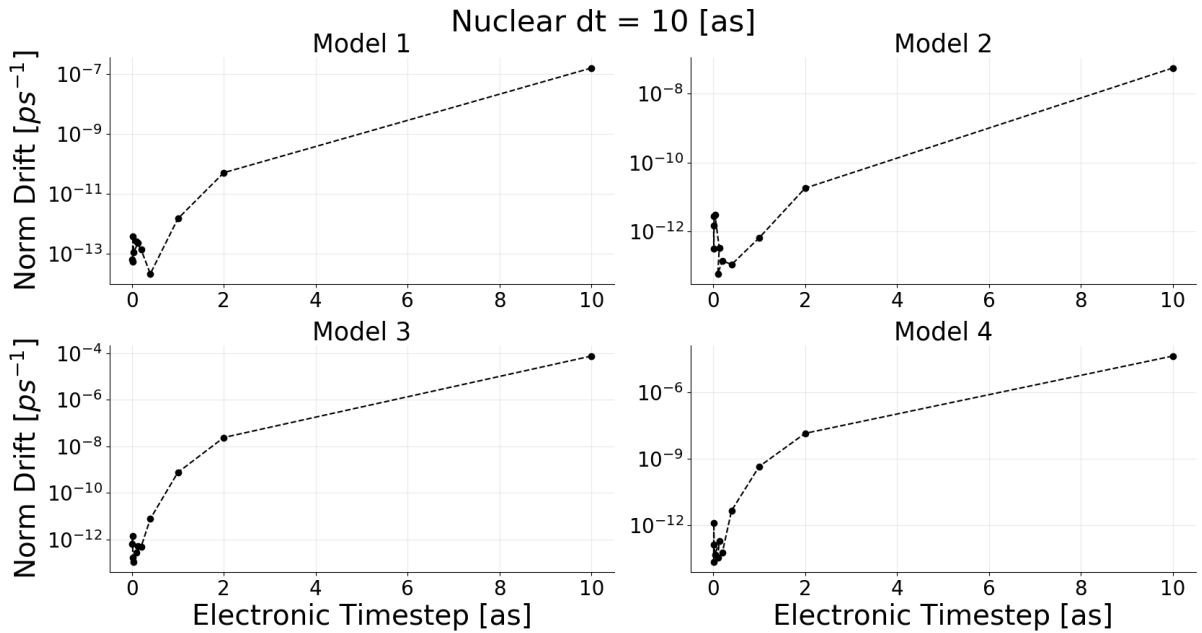


Figure 2.2: The norm conservation averaged over all replicas for Ehrenfest simulations with various electronic timesteps for each Tully model using a initial high momenta.

In appendix E, it is shown that the norm of the adiabatic expansion coefficients should be conserved throughout the simulation. To test the conservation of the norm of the expansion coefficients Ehrenfest simulations were ~~ran~~ run with various electronic timesteps (with a constant nuclear timestep) for each of the ~~4~~^{four} high momentum Tully models. The high momentum Tully models were chosen as they are expected to provide a worst case scenario of the norm conservation, due to populations changing more quickly leading to reduced sampling. As can be seen in figure 2.2, the norm of the wavefunction is conserved within numerical error (10^{-12}) when using a sufficiently small timestep in every Tully model.

2.1.2 Energy Conservation

Energy conservation is a very important property in most molecular dynamics simulations. In Ehrenfest of mean-field molecular dynamics nuclei are propagated on a population-

weighted mean potential energy surface, e.g. $\sum_k |C_{tk}^{(I)}(t)|^2 \mathbf{E}_k = E_{eff}(t)$ ⁸⁴. Kinetic energy of the classical nuclei is given by the standard formula, [e.g.](#) i.e. $\frac{1}{2}mv^2$. We can therefore write down the conserved quantity as defined below in equation (2.4):

$$\frac{dE}{dt} = \frac{d}{dt} \left[\frac{1}{2}mv^2 + \sum_k |C_{tk}^{(I)}(t)|^2 \mathbf{E}_k \right] = 0 \quad (2.4)$$

As in the norm conservation checks in section E, parameters from the high momentum cases were taken as initial conditions for simulations with various nuclear timesteps, this time holding the electronic timestep constant. The high momenta cases were chosen to show the worst case energy conservations. A linear line of best fit was then fitted to the data and the drift in the total energy (given in (2.4)) was calculated from its gradient. The results of these simulations are given in figure 2.3. In figure 2.3, we

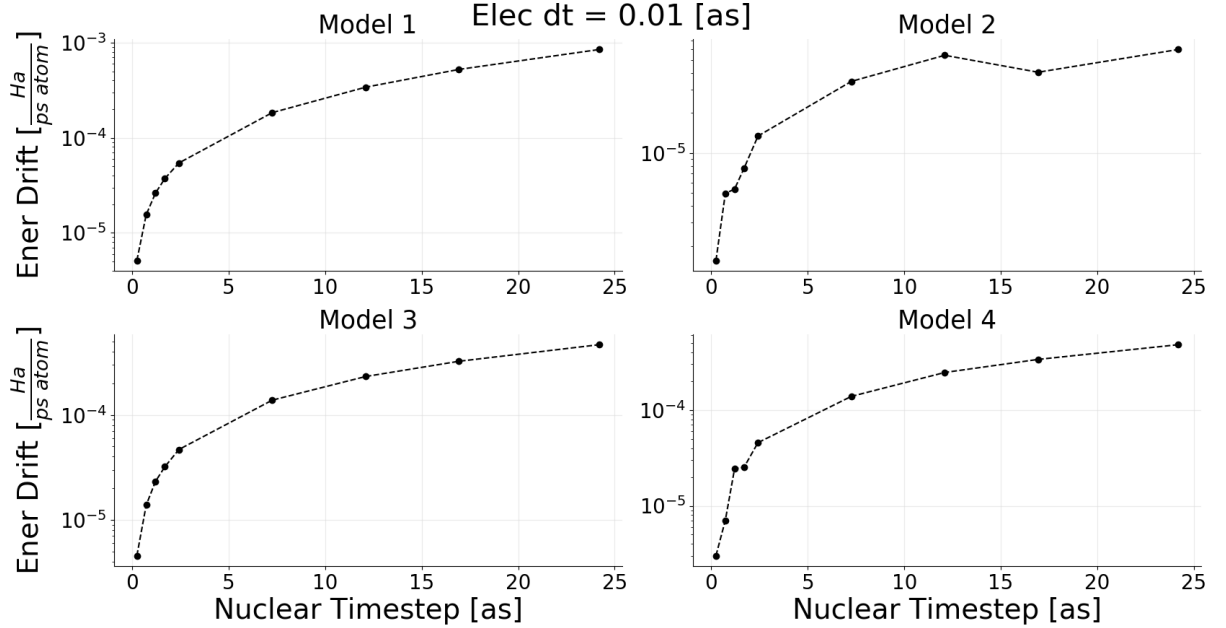


Figure 2.3: Energy conservation values for various nuclear timesteps for the high momentum case of each Tully model using Ehrenfest dynamics.

see the expected results that as the nuclear timestep is decreased the drift in the total energy also decreases. This is due to increased sampling of atomic movements leading to more continuous forces being calculated. This trend validates the implementation and shows that in the limit of infinitely small timestep (and infinite computer precision) perfect energy conservation would be achieved. However, fairly small nuclear timesteps are

required to achieve reasonable energy conservations. This is because the system contains only ~~4~~^{one} atom with a mass comparable to that of Hydrogen. If one needed an improved energy conservation a higher order integrator than the velocity verlet used here may also improve results slightly.

2.1.3 Comparisons To Literature

2.1.3.1 Gossel and Agostini

There have been ~~2~~^{two} papers published applying CTMQC and Ehrenfest to the Tully models^{2,3} and both contain results for the 4 Tully models shown in fig 2.1. The results contain data on the (ground state) adiabatic populations and a coherence indicator (shown in equation (2.5)) for ~~16~~⁸ different simulations (a low and high initial momentum simulation of Models 1, 2, 3 and 4). However, models ~~4~~^{one} and ~~4~~^{four} in Agostini² used a different initial momentum so these have been omitted from the results in figures 2.4 and 2.5. The adiabatic populations give the probability of finding the wavefunction on a particular adiabatic state and their values can range from $0 \rightarrow 1$. A value of 1 means that the wavefunction is completely localised on ~~4~~^{one} adiabatic state and there is a certainty of finding it there, and vice versa for 0. The coherence indicator gives an indication of how much ‘mixing’ has occurred between adiabatic states and can have a value from $0 \rightarrow 0.25$. A value of 0 means that the adiabatic population has completely localised on just 1 state. A value of 0.25 means that the population is equally split between the 2 states.

$$|\rho_{12}(t)|^2 = \frac{1}{N_{tr}} \sum_{I=1}^{N_{tr}} |C_1^{(I)}(t)|^2 |C_2^{(I)}(t)|^2 \quad (2.5)$$

In order to compare to results in the literature the same setup had to be used. In this case this meant sampling individual replicas’ initial conditions (positions and momenta) from a Wigner distribution with a mean position and ~~momenta~~ momentum given in appendix A. The wavefunction was initialised purely on the ground state and the same integrator was used for the nuclear and electronic propagation (velocity verlet and RK4 respectively). My results as well as the relevant data taken from Agostini and Gos-

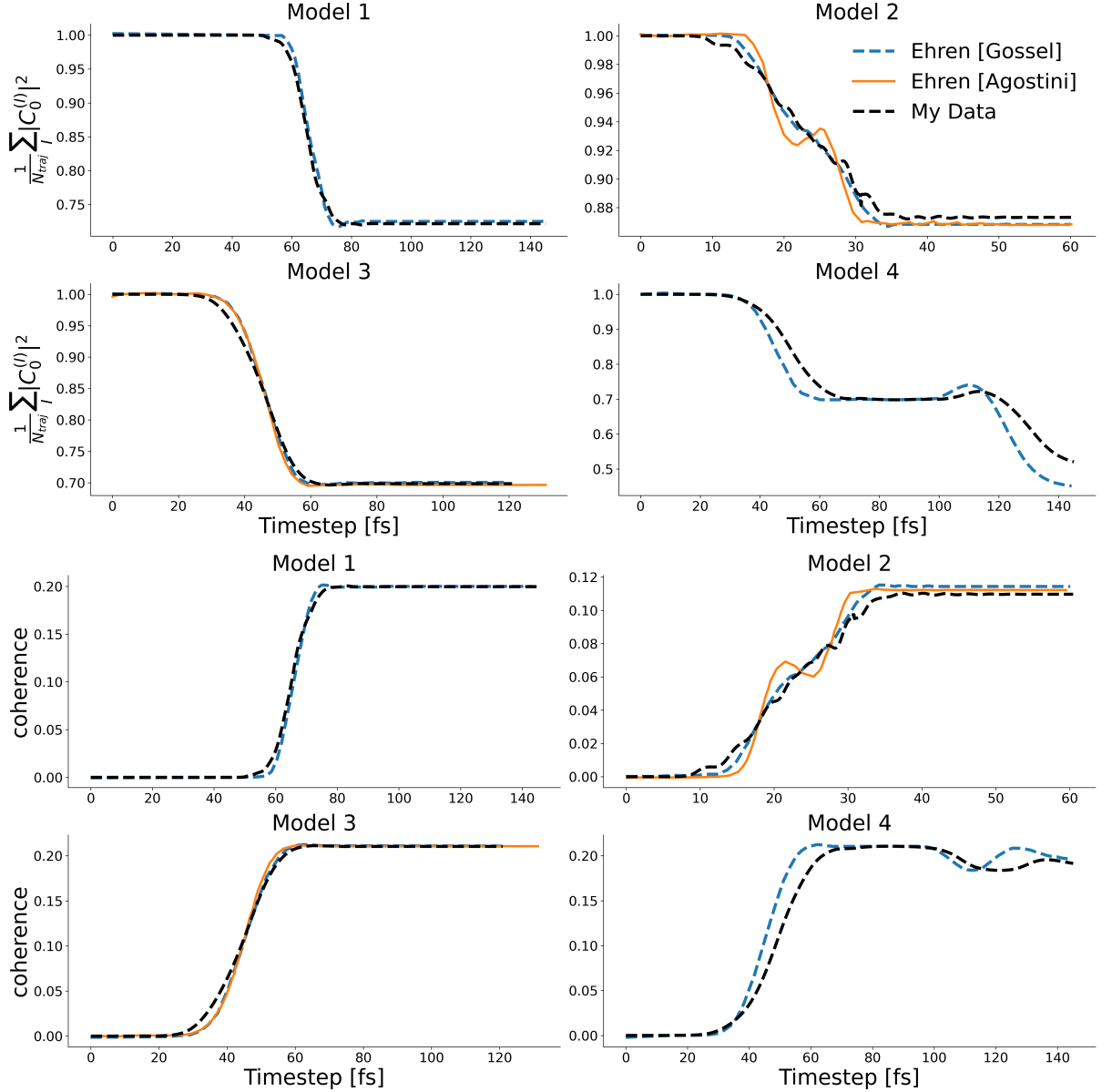


Figure 2.4: A comparison of my implementation of Ehrenfest (for 4 model Hamiltonians) and results from the literature for the low momenta cases. The black dashed lines show my data (ground state `ad_pops` adiabatic populations), the orange dashed lines are data from Agostini² and the blue solid lines are from Gossel³. The figures are labelled with their model number, whether the initial momentum was high or low and whether the populations or coherence indicator was plotted.

sel^{2,3} are shown in figures 2.4 (low momentum) and 2.5 (high momentum) for Ehrenfest dynamics. This is equivalent to full CTMQC dynamics where the quantum momentum term is set to 0. Hence, we can test most parts of the code (i.e. Runge-Kutta propagation, velocity verlet, inputs, force calculations etc...) while ignoring the new quantum

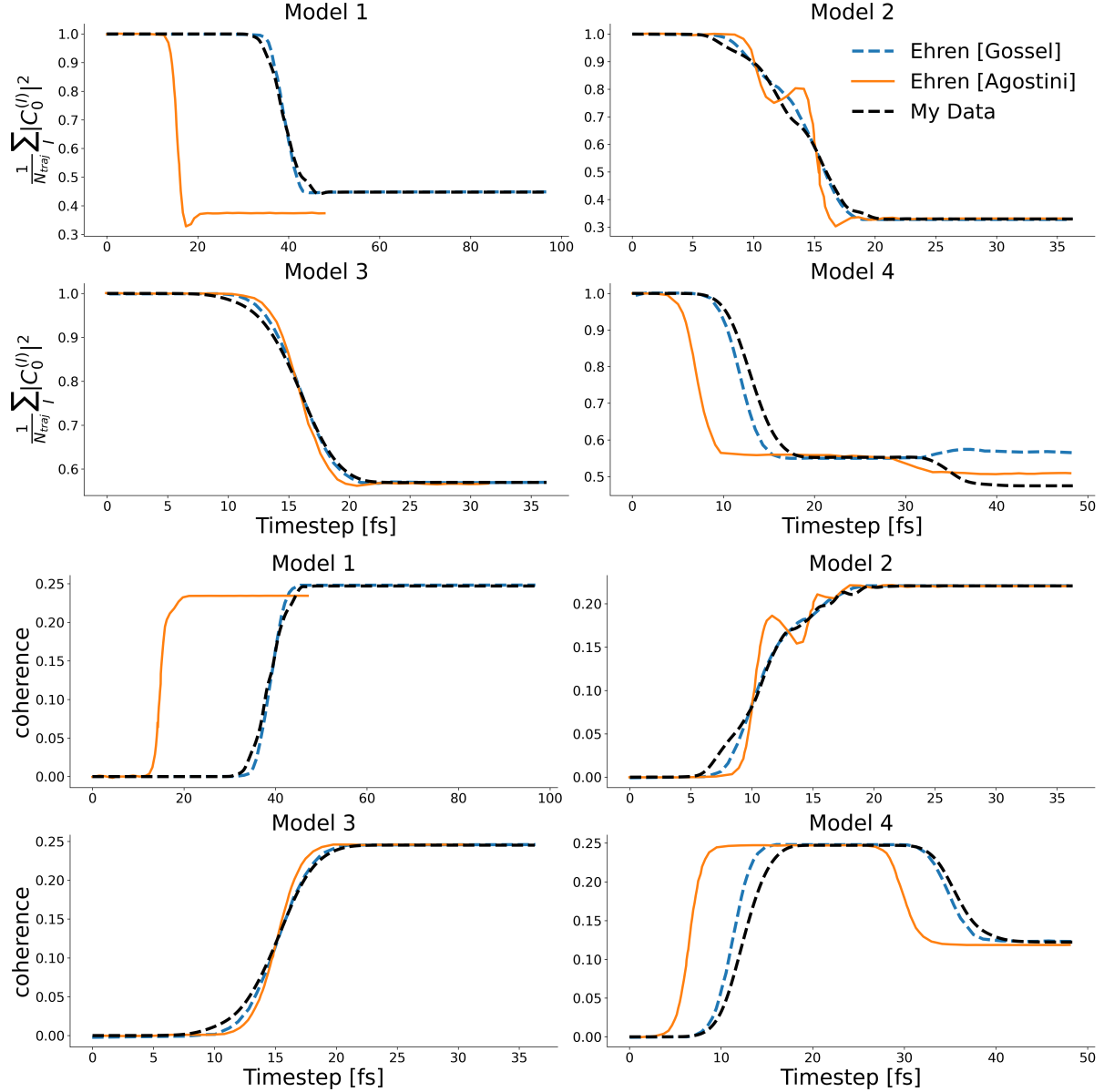


Figure 2.5: A comparison of my implementation of Ehrenfest (for 4 model Hamiltonians) and results from the literature for the high momenta cases. The black dashed lines show my data (ground state ad pops), the orange dashed lines are data from Agostini² and the blue solid lines are from Gossel³. The figures are labelled with their model number, whether the initial momentum was high or low and whether the populations or coherence indicator was plotted.

momentum and accumulated adiabatic force terms.

The results in figures 2.4 and 2.5 show that both the adiabatic populations and coherence indicator give exactly the same results as in the literature, within reasonable

error. Any deviations of results come from either a slightly different initial sampling of positions or small errors in extracting data from the graphs in each of the papers. For example, in the case of the high initial momentum simulation of model 4four all 3three results show some differences though the trend is very similar. This is true also in the Model 2 results where the Agostini populations show some transient oscillations before settling onto the same equilibrium population. This may be due to a smaller spread of positions being used in the initial sample leading to similar oscillations that aren't smoothed out in the averaging over all replicas. There are also a couple of models that start at a slightly different initial mean position in Agostini² thus they hit the nonadiabatic crossing region sooner. These are model 1one and 4four for the high momentum case.

Although not all results are exactly the same, I believe the populations agree well enough within a reasonable error to serve as a confirmation of my implementation.

2.1.3.2 Subotnik

As a final confirmation of my implementation and an investigation of the underlying physics, in a Subotnik⁸⁵, results were published for Ehrenfest simulations carried out on the 3three original Tully Models. In this work, the author presented the probabilities of the population being found transmitted through the region of nonadiabatic coupling on the ground or excited state and the probability of being reflected on the ground or upper state. In the results below, I will show comparisons of just the transmission probability onto the ground state. That is, the population that travels on the ground state beyond the region of high nonadiabatic coupling. Other probabilities will not be shown in the interest of brevity, though they agree with the published results as well as the ground state transmission in figure 2.6. As can be seen in figure 2.6 my implementation of the Ehrenfest simulation code for the Tully models agrees very well with those in Subotnik⁸⁵. The small deviation (less than 1% maximum disagreement) within each model is due to errors in retrieving data from images in original paper and possibly slightly different analysis methods. In model 1 (top-left pane) we see there is 0zero ground state population transmission below an initial momentum of around 3-4 au. This is due to the fact that the nuclei do not have enough kinetic energy to make it over the potential hill (see figure

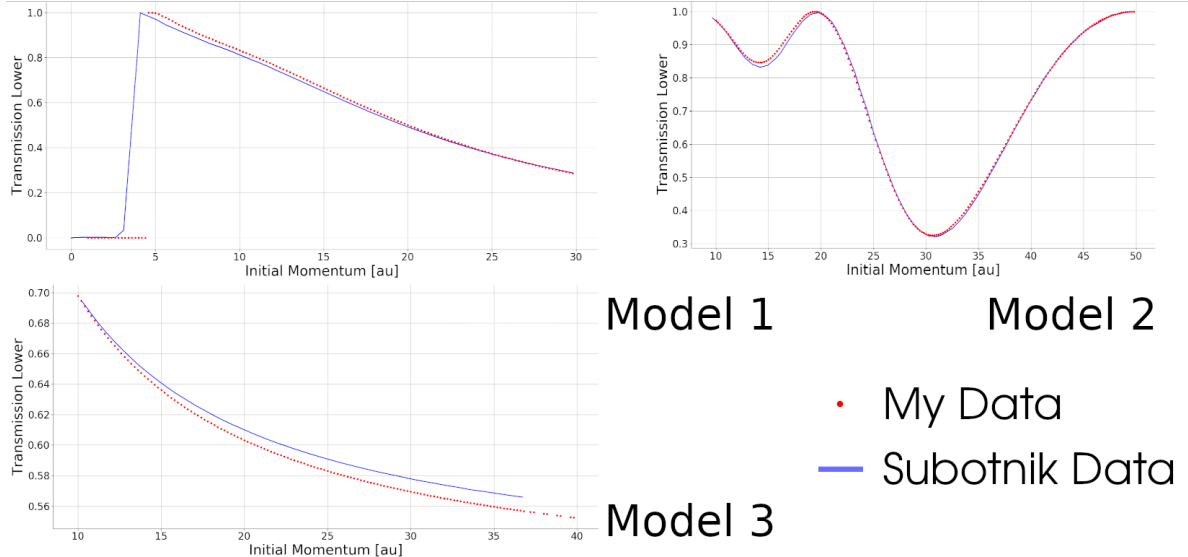


Figure 2.6: Comparison of transmission probabilities through the region of high nonadiabatic coupling on the ground state. Tully model 1 is shown in the top-left, Tully model 2 is shown in the top-right and Tully model 3 is shown in the bottom-left.

2.1) and never reach an area of high nonadiabatic coupling. The sharp cutoff is due to the classical treatment of the nuclei. In the original Subotnik⁸⁵ paper exact results were given showing the slower decay to 0_{zero} transmission with respect to initial momenta. Beyond this initial activation momentum, increases to initial momentum results in lower ground state transmissions. This is because the system has more kinetic energy allowing a higher proportion of the wavefunction to be transmitted on the excited state.

In model 2_{two} we observe St uckelberg oscillations as the atom is forced through an avoided crossing twice. During the first pass through the avoided crossing some population transfer onto the excited state occurs. In the next passage through the avoided crossing the wavefunction, now split over 2_{two} energy levels and travelling coherently, can interfere with itself. The type of interference is dependent on the velocity of the particle passing through the avoided crossings and varies in an oscillatory fashion as seen in figure 2.6.

In model 3, as the particle approaches $\mathbf{R} = 0$ it passes through a region of strong coupling, with a very small energy gap between energy levels. As the 2_{two} energy levels diverge at

$\mathbf{R} = 0$ the nonadiabatic coupling dies down to Θ_{zero} and the population remains trapped on the energy level it was on at $\mathbf{R} = 0$. Increases in initial momentum of the particle increases the likelihood that we see the particle transmit on the excited state.

These tests serve as a confirmation of the implementation of the Ehrenfest propagator. The full CTMQC equations can be implemented using the majority of the Ehrenfest infrastructure with extensions to account for the quantum momentum terms.

2.2 Testing my implementation -CTMQC

2.2.1 Conservation of the norm

In figure 2.7 only Model 3 shows a similar trend as in Ehrenfest for the norm conservation -i.e. a decreasing electronic timestep gives a rapidly decreasing norm drift. In models ~~1~~one and ~~2~~two we see that the norm drift doesn't get much better as we decrease the timestep and there are large error bars associated with each data point. In model ~~4~~four this is less pronounced but is still clearly affected. This is due to an instability in the current formalism of the quantum momentum term ($\mathcal{Q}_{lk,v}^{(I)}$).

The calculation of the quantum momentum is discussed in detail in Min, 17⁸⁰ and outlined in the introduction to the thesis in section 1.5.2. As mentioned in that section, the denominator in the expression for $\mathbf{R}_{lk,v}$ may be positive or negative and when it switches between each it can approach zero very closely. If this denominator approaches zero more quickly than the numerator then we can see large divergence in the $\mathbf{R}_{lk,v}$ term which can lead to large norm drifts. This is highlighted in figure 2.8.

2.2.1.1 Quantum Momentum Instabilities

In figure 2.8, as the denominator of quantum momentum intercept (the bottom panel) approaches Θ_{zero} the $\mathbf{R}_{lk,v}$ term may spike causing a discontinuity in the populations (through the quantum momentum). The reason this only occurs in Models 1, 2 and ~~4~~four is due to the fact that the difference in the adiabatic momenta terms ($\mathbf{f}_{l,v}^{(I)} - \mathbf{f}_{k,v}^{(I)}$) doesn't cross Θ_{zero} in Model 3 as the time-derivative of the adiabatic energies is always either positive or negative.

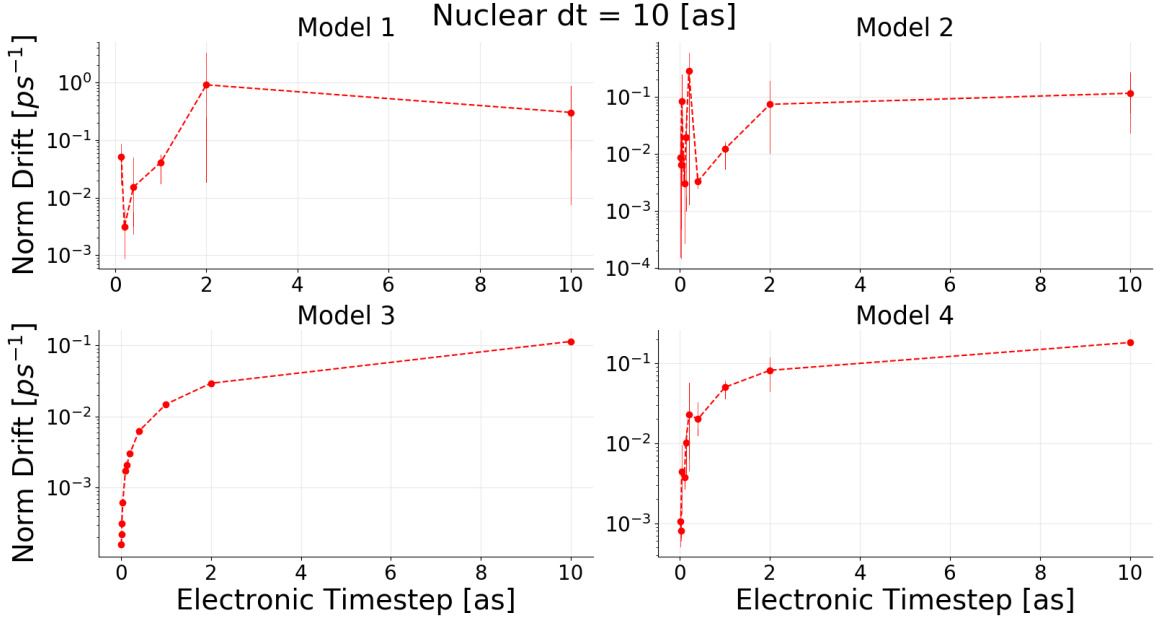


Figure 2.7: The norm conservation when using standard CTMQC as outlined in the literature for each of the Tully models. These simulations were ran with a high initial momentum. The red markers show data points and vertical bars show error bars associated with each point.

In order to correct for this divergence I have investigated a number of alterations to the calculation of the quantum momentum. These depend on the detection of the spikes/divergences in the $\mathbf{R}_{lk,v}$ term and then the appropriate treatment of them. A divergence is recorded if two conditions are met. First is a simple threshold on the time-derivative of the intercept term, i.e. $|\frac{\delta}{\delta t} \mathbf{R}_{lk,v}| > \text{thresh}$. The second condition is a threshold on the intercept denominator i.e. $|\mathbf{R}_{denom_{lk,v}}| < \text{thresh}$. For example, if the absolute time-derivative of the $\mathbf{R}_{lk,v}$ term is larger than a value (say 5) and the bottom of the fraction in equation (1.20) is within 0.01 of 0 then we assume the $\mathbf{R}_{lk,v}$ term is diverging and the simulation code then uses a different method of propagating the electronic coefficients. The alternative propagation methods that have been investigated are:

1. Use Ehrenfest Dynamics (set e.g. $\mathcal{Q}_{lk,v}$ term to 0).
2. Extrapolate the value of $\mathbf{R}_{lk,v}$ from values before the divergence (see appendix C.1).
3. Switch to using the alternative intercept $\mathbf{R}_{0,v}^{(I)}$ (see appendix C.2).

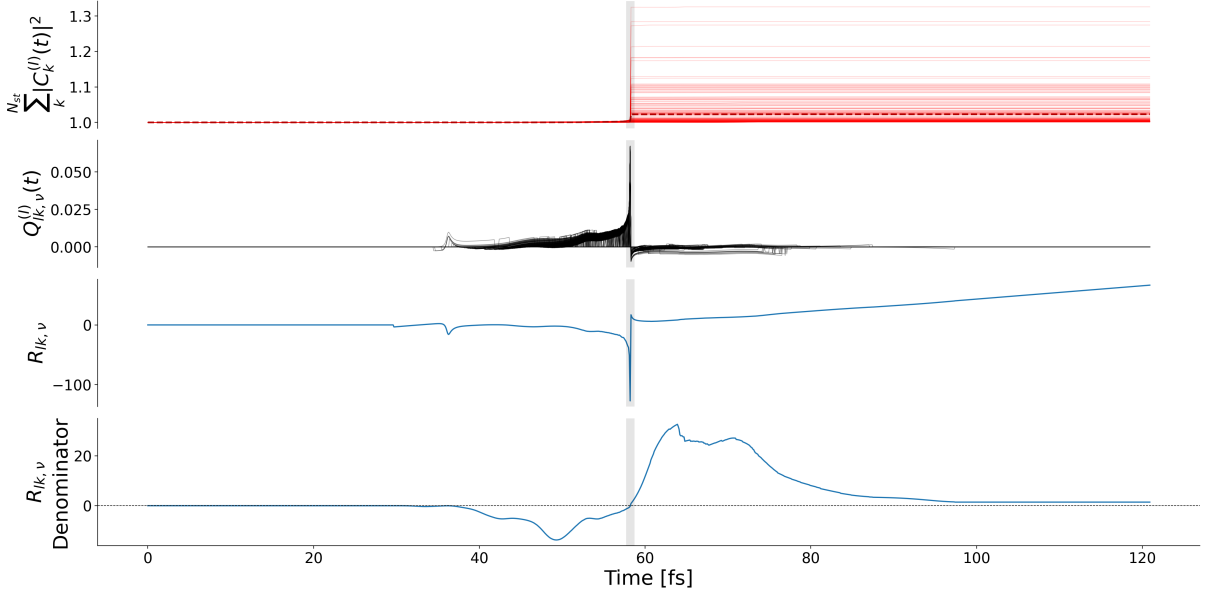


Figure 2.8: As the denominator of the $\mathbf{R}_{lk,v}$ term approaches zero (bottom panel) the full $\mathbf{R}_{lk,v}$ term (2nd to bottom panel) can approach infinity which propagates through the $\mathcal{Q}_{lk,v}^{(I)}$ term (2nd to top panel) causing discontinuities and norm drift in the populations (top panel). The grey vertical bar denotes the region the denominator approaches 0. The thin solid red lines in the top panel show the norm drift for individual replicas.

of these 3three methods, method 3three was the most successful in reducing the norm drift in the Tully Models as can be seen in figure 2.9.

In figure 2.9 we see the norm drift results after the 3 $\mathbf{R}_{lk,v}$ correction methods have been applied. The red curve shows the original data (as in figure 2.7) with its large divergences in the norm drift. The green curve shows the alternative intercept method, the blue curve shows the effect of switching to Ehrenfest during the $\mathcal{Q}_{lk,v}^{(I)}$ spikes and the black shows a method that involved extrapolating the $\mathbf{R}_{lk,v}$ value from data before the spike began. We can see clearly all 3three methods improve the norm drift, though using the alternative intercept seems to help the most. Model 3 is not affected as we do not see these divergences in the $\mathbf{R}_{lk,v}$ due to the denominator in this particular model never crossing from positive to negative (through zero). It is important to note that in each of the models with the divergence correction applied all models exhibit the expected trend of decreasing the time-step improves norm conservation. However, the norm conservation in all 4four models is still significantly higher ($\sim 7\text{-}8$ orders of magnitude) higher than that of Ehrenfest. This is due to the product of the adiabatic populations, $|C_l^{(I)}|^2|C_k^{(I)}|^2$, being

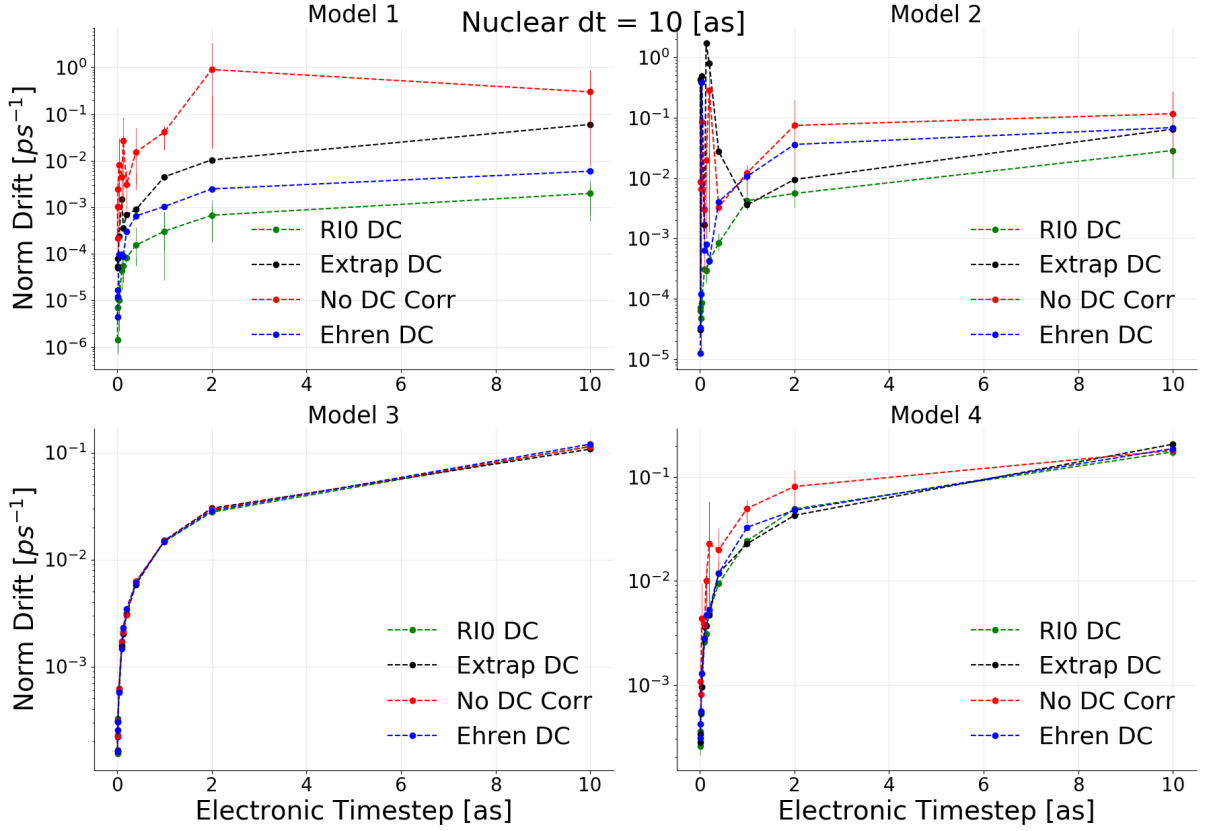


Figure 2.9: Norm conservation in CTMQC after applying a divergence correction to the $\mathbf{R}_{lk,v}$ term. RI0 refers to method 3, Extrap DC refers to method 2two and Ehren DC refers to method 1. No DC Corr shows the population norm without any corrections applied.

used in the calculation of the quantum momentum. These can be a more quickly varying quantity than just the adiabatic populations alone -thus require a smaller timestep to adequately sample in a continuous way.

2.2.2 Mathematical Tests

Multiple tests of the implementation of the quantities in the equations have been implemented in the code to ensure correct outputs. A checklist of any mathematical tests is given below:

- Checking the (anti-)symmetry of the (NACV) Hamiltonian when constructed
- Comparing the adiabatic momentum term to post-production time-integrated adiabatic energies (using trapezium rule⁸⁶)

- Checking special case solutions when all replicas are initialised at the same position such as:

- $\mathcal{Q}_{lk,v}^{(I)} = 0$
- CTMQC = Ehrenfest

- Checking special cases for when σ is replica independent (i.e. $\sigma^{(I)} = \sigma$):

- $\sigma = \frac{\hbar}{2\sigma^2}$
- $\mathbf{R}_{lk,v} = \mathbf{R}_v^{(I)} \frac{\hbar}{2\sigma^2}$ (Assuming the positions, $\mathbf{R}_v^{(I)}$ are also replica independent)

- If all adiabatic population is localised on a single state ($|C_l^{(I)}|^2 = [1, 0, 0, \dots, 0]$). Then we get Ehrenfest dynamics on that replica.
- Solving the static Schrödinger equation gives Rabi oscillation⁸⁷. See appendix D.

I have also provided 2 (more substantial) mathematical tests for the code below in the following sections.

2.2.2.1 Time Derivative of Replica-Sum of Adiabatic Populations

In the SI of Min, 17⁸⁰ a conservation equation (S27) is given. This is repeated below in equation (2.6)

$$\sum_I \mathcal{Q}_{lk,v}^{(I)}(t) \left(f_{k,v}^{(I)} - f_{l,v}^{(I)} \right) |C_k^{(I)}(t)|^2 |C_l^{(I)}(t)|^2 = 0 \quad \forall l, k, v \quad (2.6)$$

An example time-series of this quantity is given in figure 2.10 for each Tully model. The data used to calculate come from simulations of each of the Tully models using the parameters given in appendix A. No smoothing was used for the $\mathbf{R}_{lk,v}^{(I)}$ term. It can be seen in this figure that the conservation quantity hovers around Θ_{zero} for each model with a maximum deviation of 10^{-15} m_eHa.

2.2.2.2 Numerical Check of the Propagation Matrix

As the equations are currently formulated another numerical test validating the quantum momentum part of the propagation equations for the coefficients can be used. The CTMQC equation for the propagation of the adiabatic expansion coefficients is given in

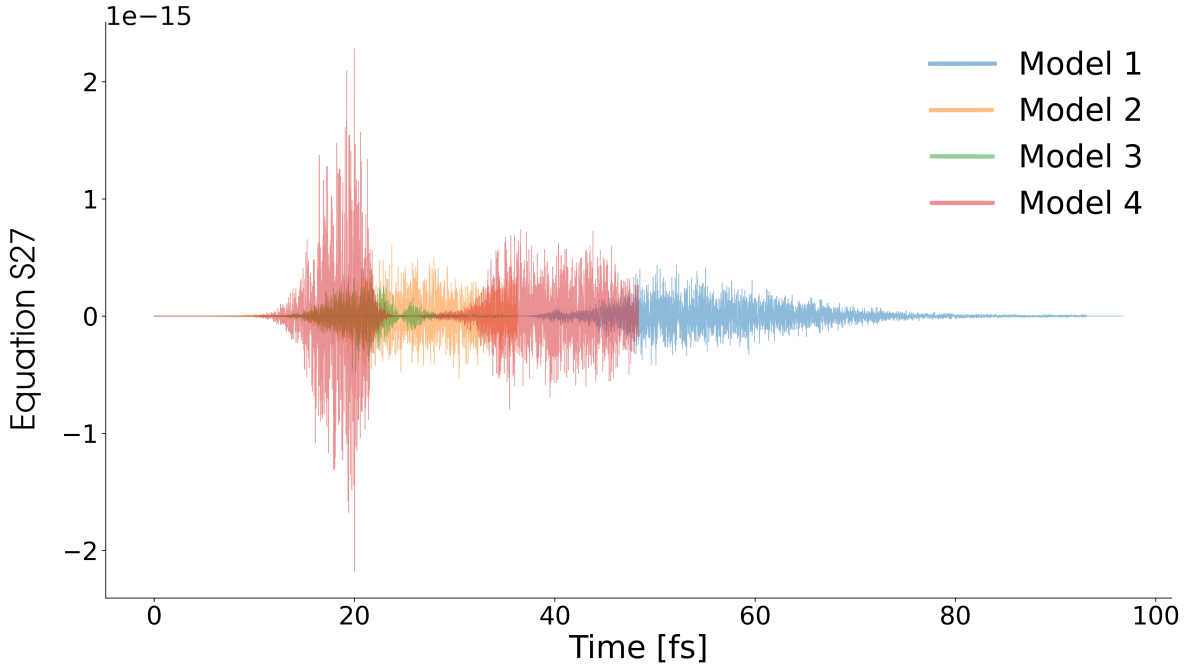


Figure 2.10: The conserved quantity given in equation (2.6) (y-axis). Each color represents data outputted by a simulation using a different model (specified in the legend). Each time-series is plotted with a translucent color meaning each model's data can be seen at once.

equation (1.15). The quantum momentum part of this equation is given below in equation (2.7).

$$\mathbb{X}_{qm,ll}^{(I)} = \sum_{v=1}^{N_n} \sum_k \frac{\mathcal{Q}_{lk,v}^{(I)}}{\hbar M_v} \cdot [\mathbf{f}_{k,v}^{(I)} - \mathbf{f}_{l,v}^{(I)}] |C_k^{(I)}|^2 \quad (2.7)$$

Where $\mathbb{X}_{qm,ll}^{(I)}$ is the diagonal matrix that, when multiplied with the adiabatic expansion coefficients, gives the quantum momentum contribution to the propagation of the expansion coefficients.

We can test the construction of this matrix within the code by multiplying by the adiabatic populations and summing as shown in equation (2.8). It can be shown, assuming perfect norm conservation, that this should equal exactly 0 -due to the symmetry of the $|C_l^{(I)}|^2 |C_k^{(I)}|^2$ and the quantum momentum matrix. This is checked for every timestep during propagation.

$$\sum_l \mathbb{X}_{qm,ll}^{(I)} |C_l^{(I)}|^2 = 0 \quad (2.8)$$

2.2.3 Energy Conservation

In Agostini² it is stated that the approximate potential energy is given by the same equation as in Ehrenfest, i.e. equation (2.4) a population weighted average of the potential energy surfaces. The 4 high momentum Tully models were simulated with various nuclear timesteps and a straight line of best fit was fitted to the total energy term.

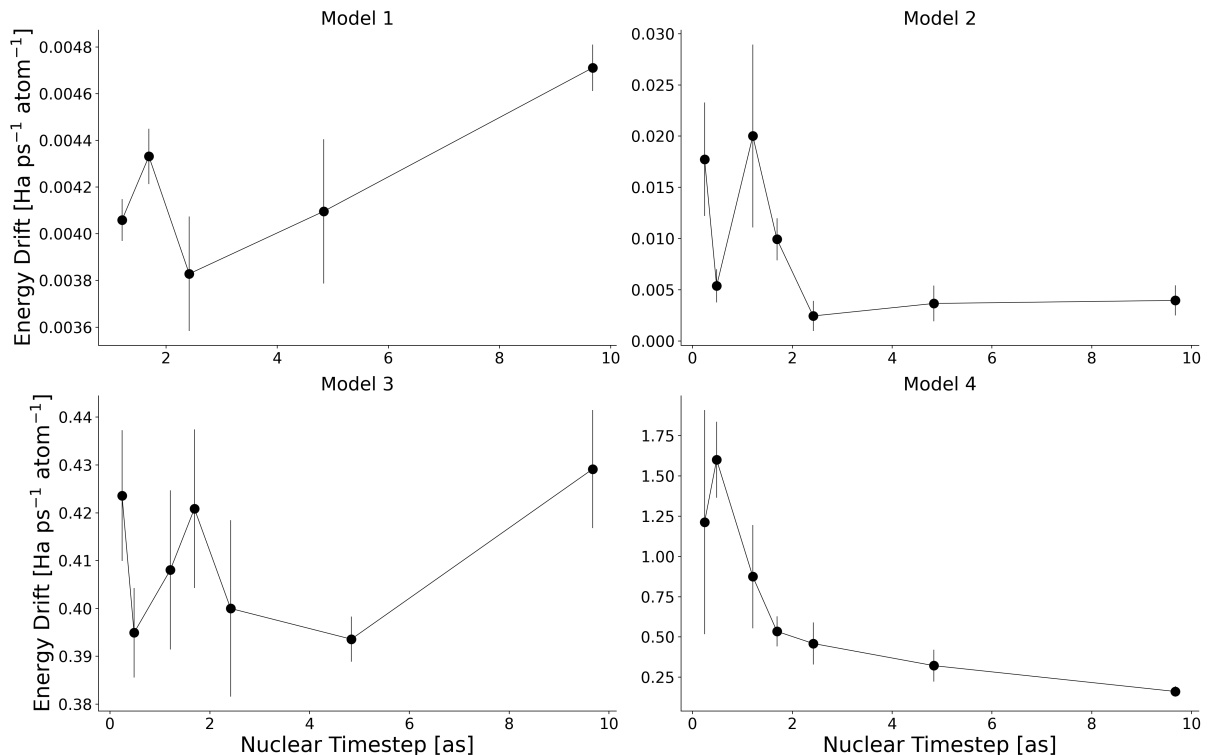


Figure 2.11: Energy drift in the 4 Tully models using the full CTMQC equations. Error bars are from multiple simulations carried out with different random sampling of the initial positions and momenta.

As can be seen in figure 2.11 the energy conservation in CTMQC does not improve with a decreasing nuclear timestep. In fact in the energy conservation worsens with decrease nuclear timestep in some models such as model 4. Additionally, in models [2two](#) and [4four](#) the errorbar increases as the timestep decreases. This is caused by an increased likelihood of coming across a divergence in the quantum momentum that can't be properly corrected, due to more steps being simulated. In model 3, the error bar stays the fairly consistent,

and the energy conservation doesn't change with respect to the timestep. In this model there are no quantum momentum divergences which means the poor energy conservation is caused by something else. The potential energy as given in Agostini² is an approximation and to achieve energy conservation comparable to Ehrenfest this may need amending.

2.2.4 Comparisons to literature

As in section 2.1.3.1 we can compare the CTMQC results to those published before in Gossel³ and Agostini². These results are given in figures 2.12 and 2.13. This time, unlike in the Ehrenfest code, we see some discrepancies between the ~~3~~three results which cannot solely be explained as small errors from different sampling of initial positions or from errors in extracting data from graphs in the papers. We can see that the errors mainly appear in the coherence indicator, looking at the bottom row in figures 2.12 and 2.5 it appears that both the Agostini and Gossel results match mine (dashed black line) very closely. The largest difference is seen in model 4, high momentum where the Gossel data and mine follow a similar trend and the Agostini data follows the exact curve more closely. The reason for this is a difference in the way the adiabatic momenta terms are handled. In the Gossel paper, a method to reset the adiabatic momenta to ~~0~~zero for each replica when the adiabatic populations collapse onto a pure adiabatic state (within a tolerance) is used. If this resetting is turned off then the populations in model ~~4~~four follow the Agostini results exactly. While resetting the adiabatic momenta worsens the calculation of the adiabatic populations in the model ~~4~~four simulations, it improves the convergence of the coherence indicator in the model 2 simulations. I will show later how using a method to dynamically alter the gaussian width parameter, used to calculate the quantum momentum, can improve the model ~~4~~four results markedly. Other deviations in results for the populations are due to a slightly different sampling of initial positions, a different handling of divergences in the quantum momentum term and constructing the $\mathcal{Q}_{lk,v}^{(I)}$ term with a different width parameter (σ) -which isn't specified in each of the paper the results have been taken from. The differences in my results and those given in the literature are on the same scale as the differences already presented in the literature and they are not large enough to invalidate my implementation. The discrepancies present between the results in the papers presented here are probably caused by the same small

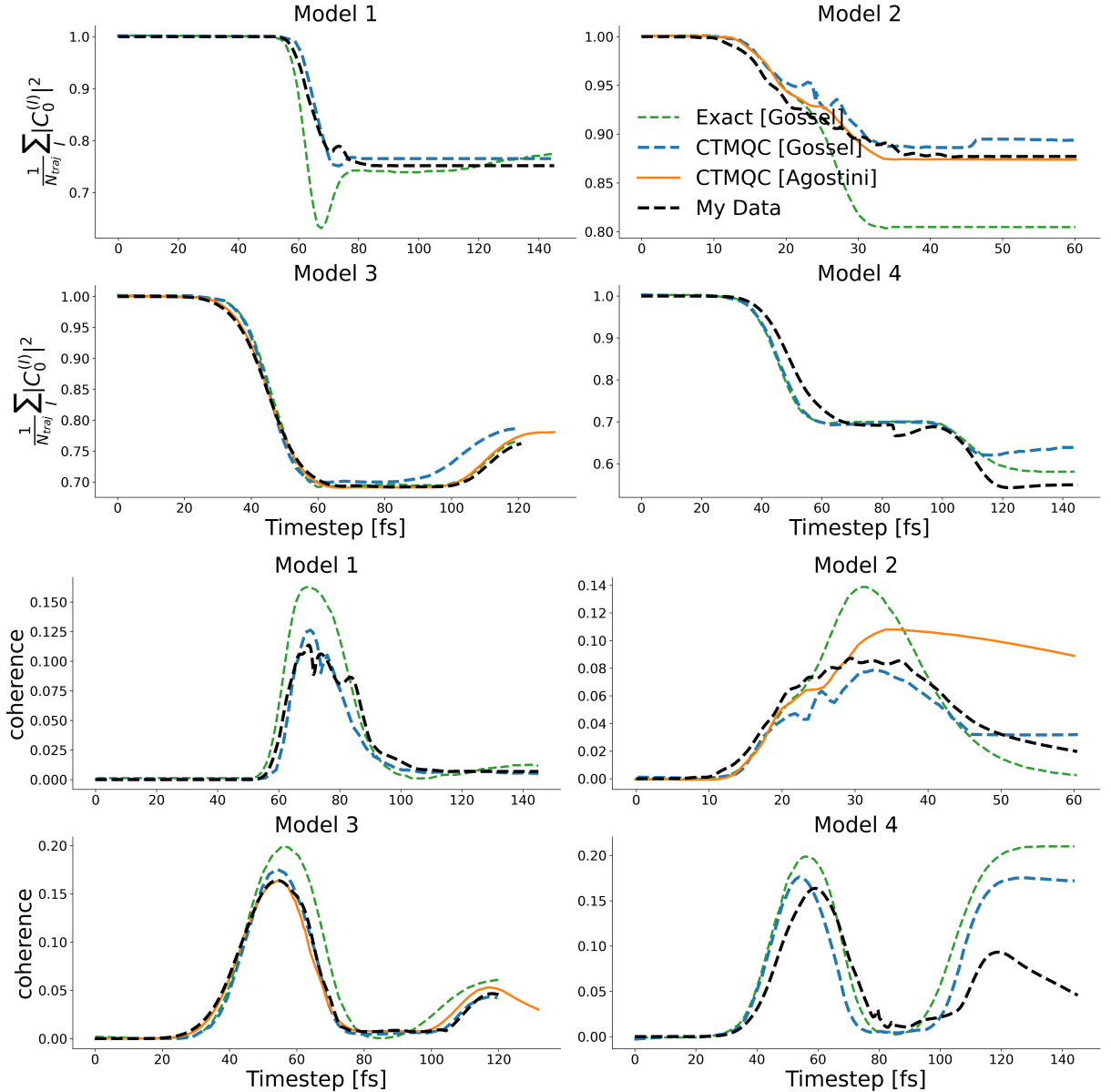


Figure 2.12: A comparison of my implementation of full CTMQC (for 4 model Hamiltonians) and results from the literature for the low momentum cases. The black dashed lines show my CTMQC data (ground state ad pops), the orange dashed lines are data from Agostini² and the blue solid lines are from Gossel³. The solid green line shows data from exact quantum mechanical simulations given in Gossel. The figures are labelled with their model number, whether the initial momentum was high or low and whether the populations or coherence indicator was plotted.

algorithmic differences causing minor discrepancies in my results. The fact many of the literature results agree exactly with my implementation can be taken as a confirmation that my implementation is working well.

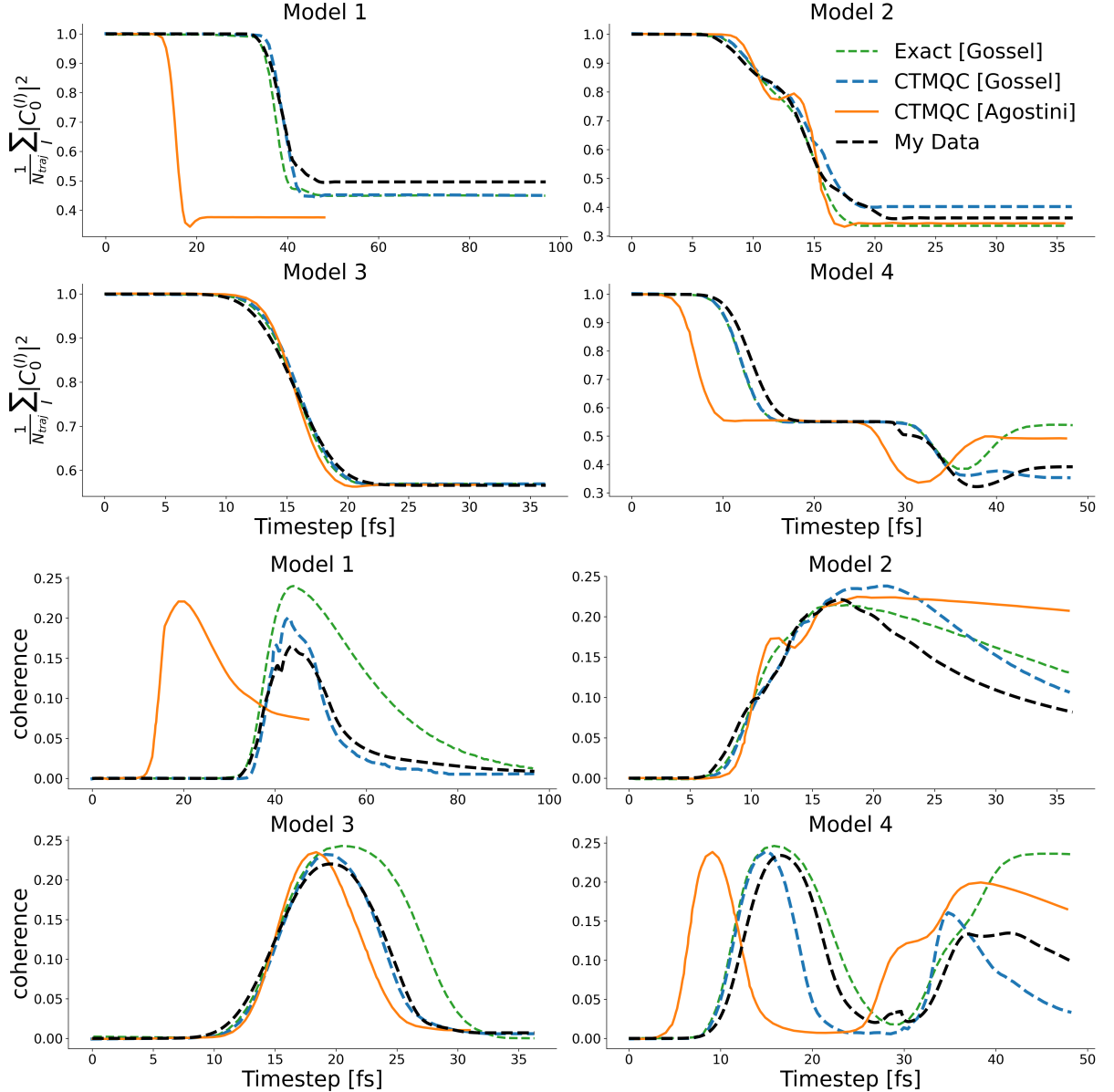


Figure 2.13: A comparison of my implementation of full CTMQC (for 4 model Hamiltonians) and results from the literature for the high momentum cases. The black dashed lines show my CTMQC data (ground state ad pops), the orange dashed lines are data from Agostini² and the blue solid lines are from Gossel³. The solid green line shows data from exact quantum mechanical simulations given in Gossel. The figures are labelled with their model number, whether the initial momentum was high or low and whether the populations or coherence indicator was plotted.

2.3 Construction of the quantum momentum

In order to calculate the quantum momentum the nuclear density must be constructed from the nuclei's positions. However, the nuclei are treated classically, i.e. as point

particles. To approximate the nuclear density from atomic positions a normal distribution is placed with the mean at position of each particle with a width of σ and combined . This method is outlined in the supplementary information on Min, 17⁸⁰ and introduces a new parameter which must be tuned in order to reproduce sensible results. If the width is too small the resulting nuclear density is too noisy and the quantum momentum values unreliable. If the width is too large the nuclear density is very smooth with little variation and the quantum momentum values become very small. Seeing as the quantum momentum is one of the most important factors affecting coherence between electronic states the careful selection of the σ parameter is important. This issue is not very well addressed in the literature. In this section I will show results of calculation carried out with various constant values of σ as well as a method for a dynamic calculation of $\sigma_v^{(I)}(t)$ on the fly. In figures 2.12 and 2.5 a constant value of 0.35 was used in order to best reproduce the results in Gossel³.

2.3.1 Constant Values of σ

The simplest option for the calculation of $\mathcal{Q}_{lk,v}^{(I)}$ is to keep the gaussian width parameter, σ , constant throughout the simulation. This also allows us to investigate the role of σ within the simulations and to determine its influence on the dynamics. To this end various simulations were carried out on the 4 Tully models with the high initial momentum. In each simulation parameters were all the same apart from the value of σ which took a value of either: 0.1, 0.2, 0.3, 0.5, 0.6, 0.75, 1 or 2 bohr. The results for these simulations are shown in figure 2.14. In this figure, we see that as the σ parameter is increased the levels of decoherence also increases. This means for larger σ values electronic populations remain in a mixed state for longer and take more time to collapse onto a single adiabatic state. Clearly, the construction of this σ parameter is important for recovery of correct electronic dynamics. Surprisingly, this doesn't seem to have much of an effect on the resulting populations. However, this is due to the fact in the limit of large σ CTMQC becomes identical to Ehrenfest dynamics and Ehrenfest dynamics captures the evolution of the adiabatic populations very well for each model, with the exception of model 4. It should also be noted that for small values of σ , propagation using CTMQC can become unstable due to a noisy nuclear density giving rise to an unstable quantum momentum term. A

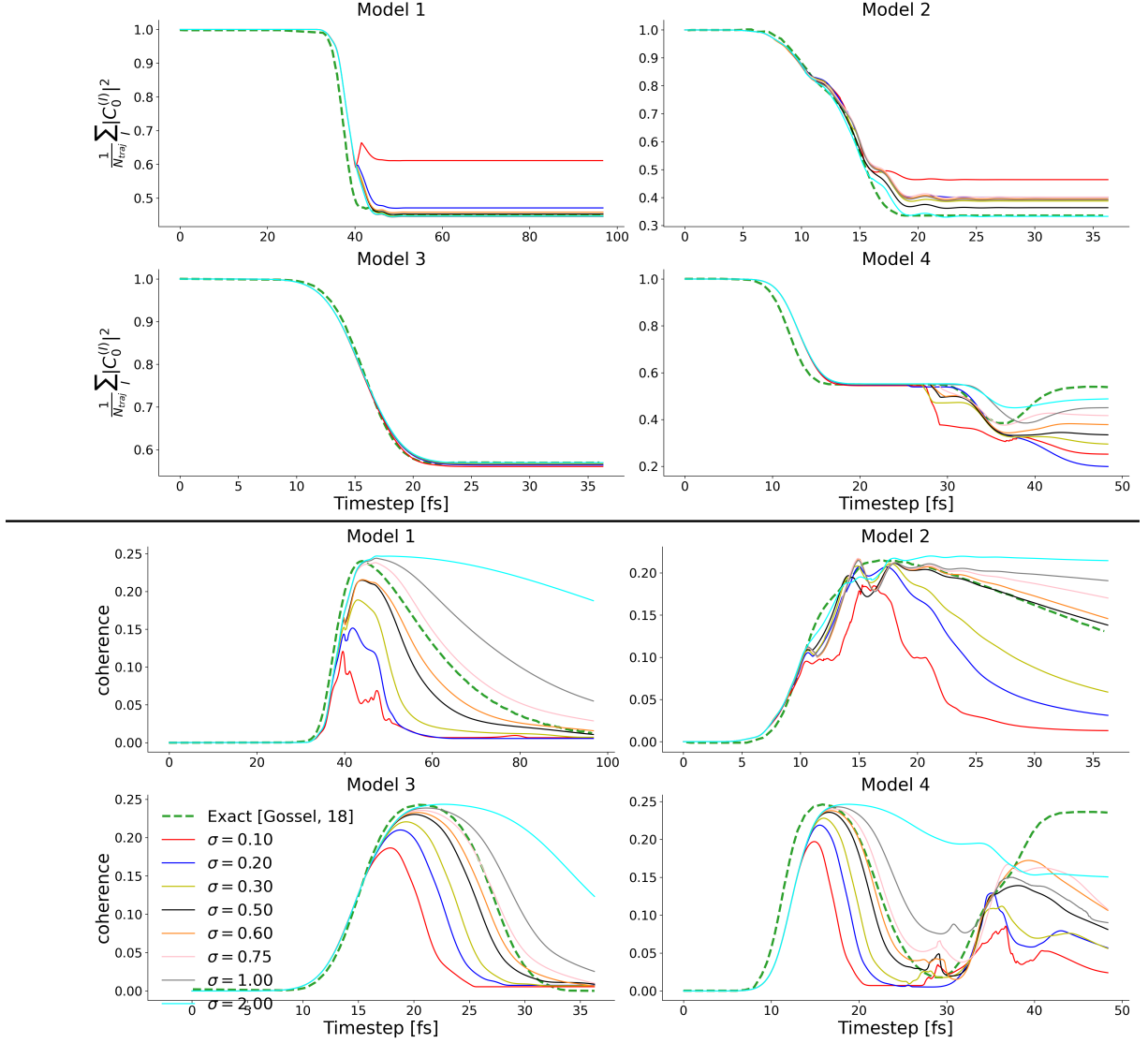


Figure 2.14: 4 high momenta cases of the Tully models with a various constant σ values used in the calculation of the quantum momentum. Thin solid lines show results from my simulations. The thick, green, dashed line shows data from exact quantum dynamics simulations taken from Gossel³ which should be taken as a reference.

value of 0.6 bohr qualitatively seems to provide the best fit to exact data. However, this may not be appropriate for all types of simulations and a deeper investigation into this parameter would be useful to investigate how general this finding is.

2.3.2 Dynamic $\sigma_v^{(I)}(t)$ calculation

In the appendix of Gossel³ an algorithm was outlined to calculate σ on-the-fly based on the density of replicas within a cutoff distance of each atom. This is given in appendix F. However, this method also relies on a constant parameter to calculate σ so doesn't

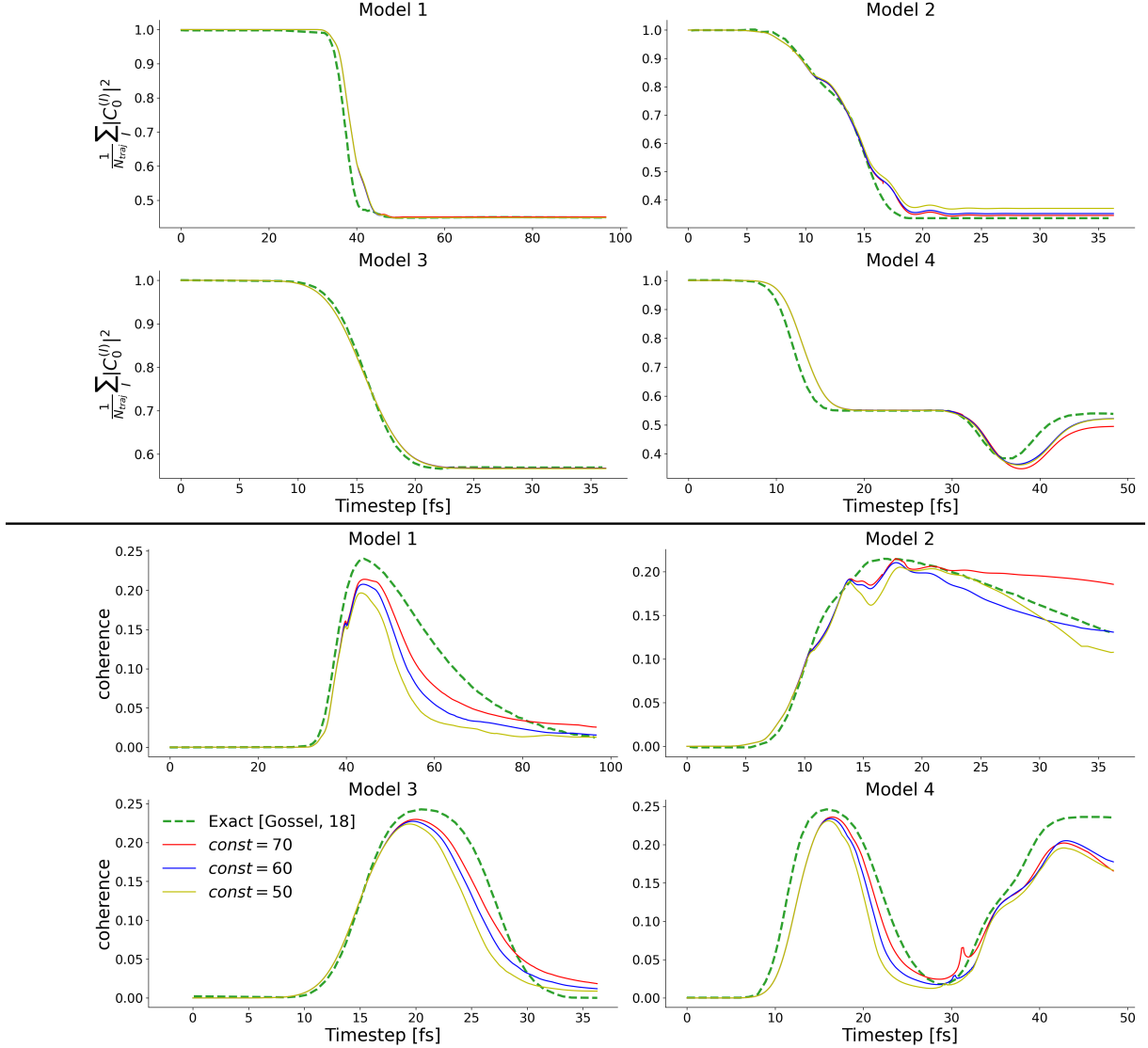


Figure 2.15

remove a parameter, though the resulting dynamics do not seem as sensitive to changes in this parameter as in σ itself.

Figure 2.15 shows populations and coherences for the 4 (high momentum) Tully models with various values of const. It is encouraging to see populations now resemble exact results more closely. This is especially true in model 4, where the dip in the populations is recovered. All 3 constants give nearly identical populations, though a constant of 60 seems to give results that most closely resemble the exact coherences. However, seeing as this (like the width parameter) is not a physical parameter it is hard to know if this is

reasonable for all systems.

2.4 Conclusion

In this chapter I have reported results from my implementation of the CTMQC equations applied to the Tully models. The Tully models are a set of 4 Hamiltonians dictating the motion of ~~1~~one atom in 1 dimension. These models are commonly simulated as they are simple enough to be solved analytically and complex enough to provide a reasonable test for any new nonadiabatic molecular dynamics (NAMD) technique. I have shown results from various tests which validate my implementation and shown how well CTMQC conserves the norm of the wavefunction and total energy, with the latter showing some concerning results. The reason for this is still unknown. I have also highlighted ~~2~~two issues with the dynamics in CTMQC. These are the sudden divergences in the quantum momentum term and the ambiguity surrounding the calculation of the gaussian width parameter, σ . The former issue has not been discussed in the literature though I have given a method designed to address it. This has been shown to significantly improve the norm conservation in the Tully model systems. The latter problem has been touched upon in the literature, though no thorough studies have been reported. I have given results for a various values of the gaussian width parameter, σ , and shown how it can affect the propagation dynamics. Further, I have implemented a method designed to dynamically update the σ parameter and benchmarked this against exact quantum dynamics simulations.

The propagation of the CTMQC equations using a model Hamiltonian is a good first step in implementing a new NAMD technique. Its relative simplicity allows for a close inspection of each of the quantities involved in the propagation, especially new quantities such as the adiabatic momentum term, $\mathbf{f}_{l,v}^{(I)}$ and the quantum momentum term, $\mathcal{Q}_{lk,v}^{(I)}$. The same code used to simulate the Tully model system can also be used as a base for future extensions such as in 3D or many atom systems. However, before such extensions are implemented a new way to construct the Hamiltonian is needed. In the next chapter I will discuss my implementation of CTMQC within the fragment orbital based framework

which relies on the fast calculation of the Hamiltonian using a finite difference method for off-diagonals and a classical force-field to calculate diagonal terms.

Bibliography

- [1] Federica Agostini, Ali Abedi, Yasumitsu Suzuki, Seung Kyu Min, Neepa T. Maitra, and E. K. U. Gross. The exact forces on classical nuclei in non-adiabatic charge transfer. *The Journal of Chemical Physics*, 142(8):084303, February 2015.
- [2] Federica Agostini, Seung Kyu Min, Ali Abedi, and E. K. U. Gross. Quantum-Classical Nonadiabatic Dynamics: Coupled- vs Independent-Trajectory Methods. *Journal of Chemical Theory and Computation*, 12(5):2127–2143, May 2016.
- [3] Graeme H. Gossel, Federica Agostini, and Neepa T. Maitra. Coupled-Trajectory Mixed Quantum-Classical Algorithm: A Deconstruction. *Journal of Chemical Theory and Computation*, August 2018.
- [4] William Humphrey, Andrew Dalke, and Klaus Schulten. VMD – Visual Molecular Dynamics. *Journal of Molecular Graphics*, 14:33–38, 1996.
- [5] John Stone. *An Efficient Library for Parallel Ray Tracing and Animation*. Master’s thesis, Computer Science Department, University of Missouri-Rolla, April 1998.
- [6] R. B. Campbell, J. M. Robertson, and J. Trotter. The crystal and molecular structure of pentacene. *Acta Crystallographica*, 14(7):705–711, Jul 1961.
- [7] R. Hesse and H. Bässler. Short-time carrier transport in amorphous pentacene. *physica status solidi (b)*, 101(2):481–487, 1980.
- [8] Jin-Hyuk Bae, Sin-Doo Lee, and Chang-Jae Yu. Deposition rate dependent mobility of an organic transistor with an anisotropic polymeric insulator. *Solid-State Electronics*, 79:98–103, 2013.

- [9] M. H. Choo, Jae Hoon Kim, and Seongil Im. Hole transport in amorphous-crystalline-mixed and amorphous pentacene thin-film transistors. *Applied Physics Letters*, 81(24):4640–4642, 2002.
- [10] D. Knipp and R.A. Street. Pentacene thin film transistors on large area compatible gate dielectrics. *Journal of Non-Crystalline Solids*, 338-340:595–598, 2004. Proceedings of the 20th International Conference on Amorphous and Microcrystalline Semiconductors.
- [11] Sandra E. Fritz, Tommie Wilson Kelley, and C. Daniel Frisbie. Effect of dielectric roughness on performance of pentacene tfts and restoration of performance with a polymeric smoothing layer. *The Journal of Physical Chemistry B*, 109(21):10574–10577, Jun 2005.
- [12] Claudia M. Duffy, Jens W. Andreasen, Dag W. Breiby, Martin M. Nielsen, Masahiko Ando, Takashi Minakata, and Henning Sirringhaus. High-mobility aligned pentacene films grown by zone-casting. *Chemistry of Materials*, 20(23):7252–7259, Dec 2008.
- [13] Hagen Klauk, Marcus Halik, Ute Zschieschang, Günter Schmid, Wolfgang Radlik, and Werner Weber. High-mobility polymer gate dielectric pentacene thin film transistors. *Journal of Applied Physics*, 92(9):5259–5263, 2002.
- [14] Yuhang Zhang, Jingsi Qiao, Si Gao, Fengrui Hu, Daowei He, Bing Wu, Ziyi Yang, Bingchen Xu, Yun Li, Yi Shi, Wei Ji, Peng Wang, Xiaoyong Wang, Min Xiao, Hangxun Xu, Jian-Bin Xu, and Xinran Wang. Probing carrier transport and structure-property relationship of highly ordered organic semiconductors at the two-dimensional limit. *Phys. Rev. Lett.*, 116:016602, Jan 2016.
- [15] J. Y. Lee, S. Roth, and Y. W. Park. Anisotropic field effect mobility in single crystal pentacene. *Applied Physics Letters*, 88(25):252106, 2006.
- [16] Yoko Takeyama, Shimpei Ono, and Yuji Matsumoto. Organic single crystal transistor characteristics of single-crystal phase pentacene grown by ionic liquid-assisted vacuum deposition. *Applied Physics Letters*, 101(8):083303, 2012.

- [17] S. Atika Arabi, Ji Dong, Misbah Mirza, Peng Yu, Liang Wang, Jun He, and Chao Jiang. Nanoseed assisted pvt growth of ultrathin 2d pentacene molecular crystal directly onto sio2 substrate. *Crystal Growth & Design*, 16(5):2624–2630, May 2016.
- [18] C. K. Chiang, C. R. Fincher, Y. W. Park, A. J. Heeger, H. Shirakawa, E. J. Louis, S. C. Gau, and Alan G. MacDiarmid. Electrical Conductivity in Doped Polyacetylene. *Physical Review Letters*, 39(17):1098–1101, October 1977.
- [19] Hideki Shirakawa, Edwin J. Louis, Alan G. MacDiarmid, Chwan K. Chiang, and Alan J. Heeger. Synthesis of electrically conducting organic polymers: halogen derivatives of polyacetylene, $(CH)_x$. *J. Chem. Soc., Chem. Commun.*, 0(16):578–580, Jan 1977.
- [20] Bernard Kippelen and Jean-Luc Brédas. Organic photovoltaics. *Energy Environ. Sci.*, 2(3):251–261, 2009.
- [21] M. J. Małachowski and J. Żmija. Organic field-effect transistors. *Opto-Electron. Rev.*, 18(2):121–136, Jun 2010.
- [22] N. Thejo Kalyani and S. J. Dhoble. Organic light emitting diodes: Energy saving lighting technology—A review. *Renewable Sustainable Energy Rev.*, 16(5):2696–2723, Jun 2012.
- [23] Sebastian Reineke, Frank Lindner, Gregor Schwartz, Nico Seidler, Karsten Walzer, Björn Lüssem, and Karl Leo. White organic light-emitting diodes with fluorescent tube efficiency. *Nature*, 459(7244):234, May 2009.
- [24] Kazuki Kato, Toshihiko Iwasaki, and Takatoshi Tsujimura. Over 130 lm/w all-phosphorescent white oleds for next-generation lighting. *Journal of Photopolymer Science and Technology*, 28:335–340, 10 2015.
- [25] Veaceslav Coropceanu, Jérôme Cornil, Demetrio A. da Silva Filho, Yoann Olivier, Robert Silbey, and Jean-Luc Brédas. Charge Transport in Organic Semiconductors. *Chemical Reviews*, 107(4):926–952, April 2007.

- [26] Samuele Giannini, Antoine Carof, Matthew Ellis, Hui Yang, Orestis George Ziogos, Soumya Ghosh, and Jochen Blumberger. Quantum localization and delocalization of charge carriers in organic semiconducting crystals. *Nature Communications*, 10(1):3843, Aug 2019.
- [27] Alessandro Troisi. Charge transport in high mobility molecular semiconductors: classical models and new theories. *Chem. Soc. Rev.*, 40:2347–2358, 2011.
- [28] Simone Fratini, Didier Mayou, and Sergio Ciuchi. The transient localization scenario for charge transport in crystalline organic materials. *Advanced Functional Materials*, 26(14):2292–2315, 2016.
- [29] I. Yavuz. Dichotomy between the band and hopping transport in organic crystals: insights from experiments. *Physical Chemistry Chemical Physics*, 19(38):25819–25828, 2017.
- [30] Tahereh Nemataram, Sergio Ciuchi, Xiaoyu Xie, Simone Fratini, and Alessandro Troisi. Practical computation of the charge mobility in molecular semiconductors using transient localization theory. *The Journal of Physical Chemistry C*, 123(12):6989–6997, Mar 2019.
- [31] S. Ciuchi, S. Fratini, and D. Mayou. Transient localization in crystalline organic semiconductors. *Phys. Rev. B*, 83:081202, Feb 2011.
- [32] Haobin Wang and Michael Thoss. A multilayer multiconfigurational time-dependent hartree study of vibrationally coupled electron transport using the scattering state representation. *The journal of physical chemistry. A*, 117, 03 2013.
- [33] Chr. Cattarius, G. A. Worth, H.-D. Meyer, and L. S. Cederbaum. All mode dynamics at the conical intersection of an octa-atomic molecule: Multi-configuration time-dependent Hartree (MCTDH) investigation on the butatriene cation. *The Journal of Chemical Physics*, 115(5):2088–2100, August 2001.
- [34] Uwe Manthe and Audrey Dell Hammerich. Wavepacket dynamics in five dimensions. photodissociation of methyl iodide. *Chemical Physics Letters*, 211(1):7–14, 1993.

- [35] U. Manthe, H.-D. Meyer, and L. S. Cederbaum. Multiconfigurational time-dependent hartree study of complex dynamics: Photodissociation of no2. *The Journal of Chemical Physics*, 97(12):9062–9071, 1992.
- [36] A. Jäckle and H.-D. Meyer. Reactive scattering using the multiconfiguration time-dependent hartree approximation: General aspects and application to the collinear h+h₂→h₂+h reaction. *The Journal of Chemical Physics*, 102(14):5605–5615, 1995.
- [37] John C. Tully. Molecular dynamics with electronic transitions. *The Journal of Chemical Physics*, 93(2):1061–1071, 1990.
- [38] P. Ehrenfest. Bemerkung über die angenäherte gültigkeit der klassischen mechanik innerhalb der quantenmechanik. *Zeitschrift für Physik*, 45(7):455–457, Jul 1927.
- [39] D. F. Coker and L. Xiao. Methods for molecular dynamics with nonadiabatic transitions. *J. Chem. Phys.*, 102(1):496–510, Jan 1995.
- [40] Guangjun Nan, Xiaodi Yang, Linjun Wang, Zhigang Shuai, and Yi Zhao. Nuclear tunneling effects of charge transport in rubrene, tetracene, and pentacene. *Phys. Rev. B*, 79:115203, Mar 2009.
- [41] Sharon Hammes-Schiffer. Theoretical Perspectives on Proton-Coupled Electron Transfer Reactions. *Acc. Chem. Res.*, 34(4):273–281, Apr 2001.
- [42] Sharon Hammes-Schiffer and John C. Tully. Proton transfer in solution: Molecular dynamics with quantum transitions. *J. Chem. Phys.*, 101(6):4657–4667, Sep 1994.
- [43] My Hang V. Huynh and Thomas J. Meyer. Proton-coupled electron transfer. *Chemical Reviews*, 107(11):5004–5064, Nov 2007.
- [44] John C. Tully. Nonadiabatic Dynamics. pages 34–71.
- [45] Simone Pisana, Michele Lazzeri, Cinzia Casiraghi, Kostya S. Novoselov, A. K. Geim, Andrea C. Ferrari, and Francesco Mauri. Breakdown of the adiabatic Born–Oppenheimer approximation in graphene. *Nat. Mater.*, 6(3):198, Feb 2007.

- [46] M. Born and R. Oppenheimer. Zur Quantentheorie der Molekeln. *Ann. Phys.*, 389(20):457–484, Jan 1927.
- [47] F Hund. *Z. Physik*, 40:742, 1927.
- [48] J Neumann and E Wigner. *Phys. Z.*, 30:467, 1929.
- [49] E Kemble and C Zener. *Phys. Rev.*, 33:536, 1929.
- [50] Clarence Zener and Ralph Howard Fowler. Non-adiabatic crossing of energy levels. *Proceedings of the Royal Society of London. Series A, Containing Papers of a Mathematical and Physical Character*, 137(833):696–702, 1932.
- [51] Xiaosong Li, John C. Tully, H. Bernhard Schlegel, and Michael J. Frisch. Ab initio Ehrenfest dynamics. *J. Chem. Phys.*, 123(8):084106, Aug 2005.
- [52] Kenichiro Saita and Dmitrii V. Shalashilin. On-the-fly ab initio molecular dynamics with multiconfigurational Ehrenfest method. *J. Chem. Phys.*, 137(22):22A506, Dec 2012.
- [53] Daniela Kohen, Frank H. Stillinger, and John C. Tully. Model studies of nonadiabatic dynamics. *J. Chem. Phys.*, 109(12):4713–4725, Sep 1998.
- [54] John C. Tully. Perspective: Nonadiabatic dynamics theory. *The Journal of Chemical Physics*, 137(22):22A301, December 2012.
- [55] Priya V. Parandekar and John C. Tully. Detailed Balance in Ehrenfest Mixed Quantum-Classical Dynamics. *Journal of Chemical Theory and Computation*, 2(2):229–235, March 2006.
- [56] Samuele Giannini, Antoine Carof, and Jochen Blumberger. Crossover from hopping to band-like charge transport in an organic semiconductor model: Atomistic nonadiabatic molecular dynamics simulation. *The Journal of Physical Chemistry Letters*, 9(11):3116–3123, Jun 2018.

- [57] Antoine Carof, Samuele Giannini, and Jochen Blumberger. Detailed balance, internal consistency, and energy conservation in fragment orbital-based surface hopping. *The Journal of Chemical Physics*, 147(21):214113, 2017.
- [58] Linjun Wang, Alexey Akimov, and Oleg V. Prezhdo. Recent progress in surface hopping: 2011–2015. *The Journal of Physical Chemistry Letters*, 7(11):2100–2112, Jun 2016.
- [59] Linjun Wang and Oleg V. Prezhdo. A simple solution to the trivial crossing problem in surface hopping. *The Journal of Physical Chemistry Letters*, 5(4):713–719, Feb 2014.
- [60] J. Spencer, F. Gajdos, and J. Blumberger. Fob-sh: Fragment orbital-based surface hopping for charge carrier transport in organic and biological molecules and materials. *The Journal of Chemical Physics*, 145(6):064102, 2016.
- [61] Fruzsina Gajdos, Siim Valner, Felix Hoffmann, Jacob Spencer, Marian Breuer, Adam Kubas, Michel Dupuis, and Jochen Blumberger. Ultrafast Estimation of Electronic Couplings for Electron Transfer between -Conjugated Organic Molecules. *Journal of Chemical Theory and Computation*, 10(10):4653–4660, October 2014.
- [62] Soumya Ghosh, Samuele Giannini, Kevin Lively, and Jochen Blumberger. Nonadiabatic dynamics with quantum nuclei: simulating charge transfer with ring polymer surface hopping. *Faraday Discuss.*, 221:501–525, 2020.
- [63] Antoine Carof, Samuele Giannini, and Jochen Blumberger. How to calculate charge mobility in molecular materials from surface hopping non-adiabatic molecular dynamics – beyond the hopping/band paradigm. *Phys. Chem. Chem. Phys.*, 21:26368–26386, 2019.
- [64] Orestis George Ziogos, Samuele Giannini, Matthew Ellis, and Jochen Blumberger. Identifying high-mobility tetracene derivatives using a non-adiabatic molecular dynamics approach. *J. Mater. Chem. C*, 8:1054–1064, 2020.

- [65] Samuele Giannini, Orestis George Ziogos, Antoine Carof, Matthew Ellis, and Jochen Blumberger. Flickering polarons extending over ten nanometres mediate charge transport in high-mobility organic crystals. *Advanced Theory and Simulations*, 3(9):2000093, 2020.
- [66] Jacob Spencer, Laura Scalfi, Antoine Carof, and Jochen Blumberger. Confronting surface hopping molecular dynamics with marcus theory for a molecular donor–acceptor system. *Faraday Discuss.*, 195:215–236, 2016.
- [67] Antoine Carof, Samuele Giannini, and Jochen Blumberger. Detailed balance, internal consistency, and energy conservation in fragment orbital-based surface hopping. *The Journal of Chemical Physics*, 147(21):214113, 2017.
- [68] J. Spencer, F. Gajdos, and J. Blumberger. Fob-sh: Fragment orbital-based surface hopping for charge carrier transport in organic and biological molecules and materials. *The Journal of Chemical Physics*, 145(6):064102, 2016.
- [69] Samuele Giannini, Orestis George Ziogos, Antoine Carof, Matthew Ellis, and Jochen Blumberger. Flickering polarons extending over ten nanometres mediate charge transport in high-mobility organic crystals. *Advanced Theory and Simulations*, 3(9):2000093, 2020.
- [70] Ali Abedi, Neepa T. Maitra, and E. K. U. Gross. Exact Factorization of the Time-Dependent Electron-Nuclear Wave Function. *Physical Review Letters*, 105(12), September 2010.
- [71] Federica Agostini, Seung Kyu Min, and E. K. U. Gross. Semiclassical analysis of the electron-nuclear coupling in electronic non-adiabatic processes. *Annalen der Physik*, 527(9-10):546–555, October 2015.
- [72] Federica Agostini, Ali Abedi, Yasumitsu Suzuki, and E.K.U. Gross. Mixed quantum-classical dynamics on the exact time-dependent potential energy surface: a fresh look at non-adiabatic processes. *Molecular Physics*, 111(22-23):3625–3640, December 2013.

- [73] Ali Abedi, Federica Agostini, Yasumitsu Suzuki, and E. K. U. Gross. Dynamical Steps that Bridge Piecewise Adiabatic Shapes in the Exact Time-Dependent Potential Energy Surface. *Physical Review Letters*, 110(26), June 2013.
- [74] Seung Kyu Min, Ali Abedi, Kwang S. Kim, and E. K. U. Gross. Is the Molecular Berry Phase an Artifact of the Born-Oppenheimer Approximation? *Phys. Rev. Lett.*, 113(26):263004, Dec 2014.
- [75] Todd J. Martínez*. Insights for Light-Driven Molecular Devices from Ab Initio Multiple Spawning Excited-State Dynamics of Organic and Biological Chromophores. *American Chemical Society*, Oct 2005.
- [76] Farnaz A. Shakib and Pengfei Huo. Ring Polymer Surface Hopping: Incorporating Nuclear Quantum Effects into Nonadiabatic Molecular Dynamics Simulations. *J. Phys. Chem. Lett.*, 8(13):3073–3080, Jul 2017.
- [77] Basile F. E. Curchod, Ivano Tavernelli, and Ursula Rothlisberger. Trajectory-based solution of the nonadiabatic quantum dynamics equations: an on-the-fly approach for molecular dynamics simulations. *PCCP*, 13(8):3231–3236, Feb 2011.
- [78] Ivano Tavernelli. Ab initio–driven trajectory-based nuclear quantum dynamics in phase space. *Phys. Rev. A*, 87(4):042501, Apr 2013.
- [79] Arne Scherrer, Federica Agostini, Daniel Sebastiani, E. K. U. Gross, and Rodolphe Vuilleumier. Nuclear velocity perturbation theory for vibrational circular dichroism: An approach based on the exact factorization of the electron-nuclear wave function. *J. Chem. Phys.*, 143(7):074106, Aug 2015.
- [80] Seung Kyu Min, Federica Agostini, Ivano Tavernelli, and E. K. U. Gross. Ab Initio Nonadiabatic Dynamics with Coupled Trajectories: A Rigorous Approach to Quantum (De)Coherence. *The Journal of Physical Chemistry Letters*, 8(13):3048–3055, July 2017.
- [81] John C. Tully. Molecular dynamics with electronic transitions. *The Journal of Chemical Physics*, 93(2):1061–1071, July 1990.

- [82] Thomas D. Kühne, Marcella Iannuzzi, Mauro Del Ben, Vladimir V. Rybkin, Patrick Seewald, Frederick Stein, Teodoro Laino, Rustam Z. Khalilullin, Ole Schütt, Florian Schiffmann, Dorothea Golze, Jan Wilhelm, Sergey Chulkov, Mohammad Hossein Bani-Hashemian, Valéry Weber, Urban Boršnik, Mathieu Taillefumier, Alice Shoshana Jakobovits, Alfio Lazzaro, Hans Pabst, Tiziano Müller, Robert Schade, Manuel Guidon, Samuel Andermatt, Nico Holmberg, Gregory K. Schenter, Anna Hehn, Augustin Bussy, Fabian Belleflamme, Gloria Tabacchi, Andreas Glöß, Michael Lass, Iain Bethune, Christopher J. Mundy, Christian Plessl, Matt Watkins, Joost VandeVondele, Matthias Krack, and Jürg Hutter. Cp2k: An electronic structure and molecular dynamics software package - quickstep: Efficient and accurate electronic structure calculations. *The Journal of Chemical Physics*, 152(19):194103, 2020.
- [83] J. Spencer, F. Gajdos, and J. Blumberger. FOB-SH: Fragment orbital-based surface hopping for charge carrier transport in organic and biological molecules and materials. *The Journal of Chemical Physics*, 145(6):064102, August 2016.
- [84] Steven L. Fiedler and Jussi Eloranta. Nonadiabatic dynamics by mean-field and surface-hopping approaches: energy conservation considerations. *Molecular Physics*, 108(11):1471–1479, 2010.
- [85] Joseph E. Subotnik. Augmented ehrenfest dynamics yields a rate for surface hopping. *The Journal of Chemical Physics*, 132(13):134112, 2010.
- [86] K.E. Atkinson. *An Introduction to Numerical Analysis*. Wiley, 1989.
- [87] R.B. Leighton Richard P. Feynman. *The Feynman Lectures on Physics, Vol 3*. Addison-Wesley, 1998.
- [88] James Kirkpatrick. An approximate method for calculating transfer integrals based on the zindo hamiltonian. *International Journal of Quantum Chemistry*, 108(1):51–56, 2008.
- [89] Harald Oberhofer and Jochen Blumberger. Revisiting electronic couplings and in-

- coherent hopping models for electron transport in crystalline c60 at ambient temperatures. *Phys. Chem. Chem. Phys.*, 14:13846–13852, 2012.
- [90] Alessandro Troisi and Giorgio Orlandi. Hole migration in dna: a theoretical analysis of the role of structural fluctuations. *The Journal of Physical Chemistry B*, 106(8):2093–2101, Feb 2002.
- [91] Adam Kubas, Felix Hoffmann, Alexander Heck, Harald Oberhofer, Marcus Elstner, and Jochen Blumberger. Electronic couplings for molecular charge transfer: Benchmarking cdft, fodft, and fodftb against high-level ab initio calculations. *The Journal of Chemical Physics*, 140(10):104105, 2014.
- [92] Adam Kubas, Fruzsina Gajdos, Alexander Heck, Harald Oberhofer, Marcus Elstner, and Jochen Blumberger. Electronic couplings for molecular charge transfer: benchmarking cdft, fodft and fodftb against high-level ab initio calculations. ii. *Phys. Chem. Chem. Phys.*, 17:14342–14354, 2015.
- [93] Antoine Carof, Samuele Giannini, and Jochen Blumberger. Detailed balance, internal consistency, and energy conservation in fragment orbital-based surface hopping. *The Journal of Chemical Physics*, 147(21):214113, December 2017.
- [94] Fruzsina Gajdos, Siim Valner, Felix Hoffmann, Jacob Spencer, Marian Breuer, Adam Kubas, Michel Dupuis, and Jochen Blumberger. Ultrafast estimation of electronic couplings for electron transfer between π -conjugated organic molecules. *Journal of Chemical Theory and Computation*, 10(10):4653–4660, Oct 2014.
- [95] T.P. Nguyen. Defect analysis in organic semiconductors. *Materials Science in Semiconductor Processing*, 9(1):198 – 203, 2006. 11th International Conference on Defects - Recognition Imaging and Physics in Semiconductors (DRIP-XI) Sept. 13-19 in Beijing.
- [96] Biswajit Ray, Aditya G. Baradwaj, Bryan W. Boudouris, and Muhammad A. Alam. Defect characterization in organic semiconductors by forward bias capacitance–voltage (fb-cv) analysis. *The Journal of Physical Chemistry C*, 118(31):17461–17466, Aug 2014.

- [97] W. S. Hu, Y. T. Tao, Y. J. Hsu, D. H. Wei, and Y. S. Wu. Molecular orientation of evaporated pentacene films on gold: alignment effect of self-assembled monolayer. *Langmuir*, 21(6):2260–2266, Mar 2005.
- [98] Tatsuo Hasegawa and Jun Takeya. Organic field-effect transistors using single crystals. *Science and Technology of Advanced Materials*, 10(2):024314, 2009.
- [99] John E. Anthony, James S. Brooks, David L. Eaton, and Sean R. Parkin. Functionalized pentacene: improved electronic properties from control of solid-state order. *Journal of the American Chemical Society*, 123(38):9482–9483, Sep 2001.
- [100] John E. Anthony, David L. Eaton, and Sean R. Parkin. A road map to stable, soluble, easily crystallized pentacene derivatives. *Organic Letters*, 4(1):15–18, Jan 2002.
- [101] A. D’Angelo, B. Edgar, A. P. Hurt, and M. D. Antonijević. Physico-chemical characterisation of three-component co-amorphous systems generated by a melt-quench method. *Journal of Thermal Analysis and Calorimetry*, 134(1):381–390, Oct 2018.
- [102] Wanderlã L. Scopel, Antônio J. R. da Silva, and A. Fazzio. Amorphous hfo_2 and $\text{hf}_{1-x}\text{si}_x\text{O}$ via a melt-and-quench scheme using ab initio molecular dynamics. *Phys. Rev. B*, 77:172101, May 2008.
- [103] Seth S. Berbano, Inseok Seo, Christian M. Bischoff, Katherine E. Schuller, and Steve W. Martin. Formation and structure of $\text{na}_2\text{s}+\text{p}_2\text{s}_5$ amorphous materials prepared by melt-quenching and mechanical milling. *Journal of Non-Crystalline Solids*, 358(1):93 – 98, 2012.
- [104] Pranav Karmwar, Kirsten Graeser, Keith C. Gordon, Clare J. Strachan, and Thomas Rades. Investigation of properties and recrystallisation behaviour of amorphous indomethacin samples prepared by different methods. *International Journal of Pharmaceutics*, 417(1):94 – 100, 2011. Advanced characterization techniques.
- [105] Min-Jin Ko, Joel Plawsky, and Meyer Birnboim. Fabrication of cds/ag hybrid

- quantum dot composites using a melt/quench method. Journal of Non-Crystalline Solids, 203:211 – 216, 1996. Optical and Electrical Propertias of Glasses.
- [106] Steve Plimpton. Fast parallel algorithms for short-range molecular dynamics. Journal of Computational Physics, 117(1):1 – 19, 1995.
- [107] Steve Plimpton. Lammps software. <http://lammps.sandia.gov>, 1995. [Online; accessed 21-Jan-2021].
- [108] Steve Plimpton, Roy Pollock, and Mark Stevens. Particle-mesh ewald and rRESPA for parallel molecular dynamics simulations. In In Proceedings of the Eighth SIAM Conference on Parallel Processing for Scientific Computing, 1997.
- [109] Christopher I. Bayly, Piotr Cieplak, Wendy Cornell, and Peter A. Kollman. A well-behaved electrostatic potential based method using charge restraints for deriving atomic charges: the resp model. The Journal of Physical Chemistry, 97(40):10269–10280, Oct 1993.
- [110] M. J. Frisch, G. W. Trucks, H. B. Schlegel, G. E. Scuseria, M. A. Robb, J. R. Cheeseman, G. Scalmani, V. Barone, G. A. Petersson, H. Nakatsuji, X. Li, M. Caricato, A. V. Marenich, J. Bloino, B. G. Janesko, R. Gomperts, B. Mennucci, H. P. Hratchian, J. V. Ortiz, A. F. Izmaylov, J. L. Sonnenberg, D. Williams-Young, F. Ding, F. Lipparini, F. Egidi, J. Goings, B. Peng, A. Petrone, T. Henderson, D. Ranasinghe, V. G. Zakrzewski, J. Gao, N. Rega, G. Zheng, W. Liang, M. Hada, M. Ehara, K. Toyota, R. Fukuda, J. Hasegawa, M. Ishida, T. Nakajima, Y. Honda, O. Kitao, H. Nakai, T. Vreven, K. Throssell, J. A. Montgomery, Jr., J. E. Peralta, F. Ogliaro, M. J. Bearpark, J. J. Heyd, E. N. Brothers, K. N. Kudin, V. N. Staroverov, T. A. Keith, R. Kobayashi, J. Normand, K. Raghavachari, A. P. Rendell, J. C. Burant, S. S. Iyengar, J. Tomasi, M. Cossi, J. M. Millam, M. Klene, C. Adamo, R. Cammi, J. W. Ochterski, R. L. Martin, K. Morokuma, O. Farkas, J. B. Foresman, and D. J. Fox. Gaussian~16 Revision C.01, 2016. Gaussian Inc. Wallingford CT.

- [111] Axel D Becke. Becke's three parameter hybrid method using the lyp correlation functional. *J. Chem. Phys.*, 98(492):5648–5652, 1993.
- [112] C Lee, W Yang, and RG Parr. Density-functional exchange-energy approximation with correct asymptotic behaviour. *Phys. Rev. B*, 37(2):785–789, 1988.
- [113] Junmei Wang, Romain M. Wolf, James W. Caldwell, Peter A. Kollman, and David A. Case. Development and testing of a general amber force field. *Journal of Computational Chemistry*, 25(9):1157–1174, 2004.
- [114] Makoto Yoneya, Masahiro Kawasaki, and Masahiko Ando. Molecular dynamics simulations of pentacene thin films: The effect of surface on polymorph selection. *J. Mater. Chem.*, 20:10397–10402, 2010.
- [115] Makoto Yoneya, Masahiro Kawasaki, and Masahiko Ando. Are pentacene monolayer and thin-film polymorphs really substrate-induced? a molecular dynamics simulation study. *The Journal of Physical Chemistry C*, 116(1):791–795, Jan 2012.
- [116] Makoto Yoneya. Simulation of crystallization of pentacene and its derivatives from solution. *The Journal of Physical Chemistry C*, Jan 2021.
- [117] Ryan A. Miller, Amanda Larson, and Karsten Pohl. Novel surface diffusion characteristics for a robust pentacene derivative on au(111) surfaces. *Chemical Physics Letters*, 678:28 – 34, 2017.
- [118] Dong Wang, Ling Tang, Mengqiu Long, and Zhigang Shuai. Anisotropic thermal transport in organic molecular crystals from nonequilibrium molecular dynamics simulations. *The Journal of Physical Chemistry C*, 115(13):5940–5946, Apr 2011.
- [119] Florian Steiner, Carl Poelking, Dorota Niedzialek, Denis Andrienko, and Jenny Nelson. Influence of orientation mismatch on charge transport across grain boundaries in tri-isopropylsilyl ethynyl (tips) pentacene thin films. *Phys. Chem. Chem. Phys.*, 19:10854–10862, 2017.

- [120] Ida Bagus Hendra Prastiawan, Jingxiang Xu, Yusuke Ootani, Yuji Higuchi, Nobuki Ozawa, Shingo Maruyama, Yuji Matsumoto, and Momoji Kubo. Molecular interactions between pentacene and imidazolium ionic liquids: A molecular dynamics study. *Chemistry Letters*, 47(9):1154–1157, 2018.
- [121] Martin Ester, Hans-Peter Kriegel, Jörg Sander, and Xiaowei Xu. A density-based algorithm for discovering clusters in large spatial databases with noise. pages 226–231. AAAI Press, 1996.
- [122] EPA DSSTox. Epa dsstox. <https://comptox.epa.gov/dashboard/DTXSID7059648>, 2021. [Online; accessed 25-Jan-2021].
- [123] Stefan Schiefer, Martin Huth, Alexander Dobrinevski, and Bert Nickel. Determination of the crystal structure of substrate-induced pentacene polymorphs in fiber structured thin films. *Journal of the American Chemical Society*, 129(34):10316–10317, Aug 2007.
- [124] M. Klues and G. Witte. Crystalline packing in pentacene-like organic semiconductors. *CrystEngComm*, 20:63–74, 2018.
- [125] Sean M. Ryno, Chad Risko, and Jean-Luc Brédas. Impact of molecular packing on electronic polarization in organic crystals: The case of pentacene vs tips-pentacene. *Journal of the American Chemical Society*, 136(17):6421–6427, Apr 2014.
- [126] Daniel Käfer, Mira El Helou, Christian Gemel, and Gregor Witte. Packing of planar organic molecules: Interplay of van der waals and electrostatic interaction. *Crystal Growth & Design*, 8(8):3053–3057, Aug 2008.
- [127] Thorsten Vehoff, Yeon Sook Chung, Karen Johnston, Alessandro Troisi, Do Y. Yoon, and Denis Andrienko. Charge transport in self-assembled semiconducting organic layers: Role of dynamic and static disorder. *The Journal of Physical Chemistry C*, 114(23):10592–10597, Jun 2010.
- [128] Wei-Qiao Deng and William A. Goddard. Predictions of hole mobilities in oligoacene

- organic semiconductors from quantum mechanical calculations. *The Journal of Physical Chemistry B*, 108(25):8614–8621, Jun 2004.
- [129] Joe J. Kwiatkowski, Jarvist M. Frost, and Jenny Nelson. The effect of morphology on electron field-effect mobility in disordered c_{60} thin films. *Nano Letters*, 9(3):1085–1090, Mar 2009.
- [130] Stavros Athanasopoulos, James Kirkpatrick, Diego Martínez, Jarvist M. Frost, Clare M. Foden, Alison B. Walker, and Jenny Nelson. Predictive study of charge transport in disordered semiconducting polymers. *Nano Letters*, 7(6):1785–1788, Jun 2007.
- [131] Thorsten Vehoff, Björn Baumeier, Alessandro Troisi, and Denis Andrienko. Charge transport in organic crystals: Role of disorder and topological connectivity. *Journal of the American Chemical Society*, 132(33):11702–11708, Aug 2010.
- [132] Pascal Kordt and Denis Andrienko. Modeling of spatially correlated energetic disorder in organic semiconductors. *Journal of Chemical Theory and Computation*, 12(1):36–40, Jan 2016.
- [133] Yuan Zhang, Ling-Kun Meng, Jin Hu, Rui-Ke Zou, Chao Tang, Gong Li, Yan Ding, Hai-Tong Cai, Zhi-Yao Yang, and Wei Huang. Theoretical exploration of carrier dynamics in amorphous pyrene–fluorene derivative organic semiconductors. *ACS Omega*, 4(9):14124–14132, Aug 2019.
- [134] Orestis George Ziogos, Samuele Giannini, Matthew Ellis, and Jochen Blumberger. Identifying high-mobility tetracene derivatives using a non-adiabatic molecular dynamics approach. *J. Mater. Chem. C*, 8:1054–1064, 2020.
- [135] Nicolas G. Martinelli, Matteo Savini, Luca Muccioli, Yoann Olivier, Frédéric Castet, Claudio Zannoni, David Beljonne, and Jérôme Cornil. Modeling polymer dielectric/pentacene interfaces: On the role of electrostatic energy disorder on charge carrier mobility. *Advanced Functional Materials*, 19(20):3254–3261, 2009.

- [136] P. P. Ewald. Die berechnung optischer und elektrostatischer gitterpotentiale. *Annalen der Physik*, 369(3):253–287, 1921.
- [137] Abdulnour Y. Toukmaji and John A. Board. Ewald summation techniques in perspective: a survey. *Computer Physics Communications*, 95(2):73–92, 1996.
- [138] D. Wolf, P. Kebinski, S. R. Phillpot, and J. Eggebrecht. Exact method for the simulation of coulombic systems by spherically truncated, pairwise $r-1$ summation. *The Journal of Chemical Physics*, 110(17):8254–8282, 1999.
- [139] Dirk Zahn, Bernd Schilling, and Stefan M. Kast. Enhancement of the wolf damped coulomb potential: static, dynamic, and dielectric properties of liquid water from molecular simulation. *The Journal of Physical Chemistry B*, 106(41):10725–10732, Oct 2002.
- [140] Christopher J. Fennell and J. Daniel Gezelter. Is the ewald summation still necessary? pairwise alternatives to the accepted standard for long-range electrostatics. *The Journal of Chemical Physics*, 124(23):234104, 2006.
- [141] Colin R. Groom, Ian J. Bruno, Matthew P. Lightfoot, and Suzanna C. Ward. The Cambridge Structural Database. *Acta Crystallographica Section B*, 72(2):171–179, Apr 2016.
- [142] Pavlo O. Dral, Mario Barbatti, and Walter Thiel. Nonadiabatic excited-state dynamics with machine learning. *The Journal of Physical Chemistry Letters*, 9(19):5660–5663, Oct 2018.
- [143] Zhigang Shuai, Hua Geng, Wei Xu, Yi Liao, and Jean-Marie André. From charge transport parameters to charge mobility in organic semiconductors through multiscale simulation. *Chem. Soc. Rev.*, 43:2662–2679, 2014.
- [144] Weiwei Xie, Daniel Holub, Tomáš Kubář, and Marcus Elstner. Performance of mixed quantum-classical approaches on modeling the crossover from hopping to bandlike charge transport in organic semiconductors. *Journal of Chemical Theory and Computation*, 16(4):2071–2084, Apr 2020.

- [145] Sebastian T. Hoffmann, Stavros Athanasopoulos, David Beljonne, Heinz Bässler, and Anna Köhler. How do triplets and charges move in disordered organic semiconductors? a monte carlo study comprising the equilibrium and nonequilibrium regime. *The Journal of Physical Chemistry C*, 116(31):16371–16383, Aug 2012.
- [146] Hua Geng, Qian Peng, Linjun Wang, Haijiao Li, Yi Liao, Zhiying Ma, and Zhigang Shuai. Toward quantitative prediction of charge mobility in organic semiconductors: Tunneling enabled hopping model. *Advanced Materials*, 24(26):3568–3572, 2012.
- [147] Nianduan Lu, Ling Li, Writam Banerjee, Pengxiao Sun, Nan Gao, and Ming Liu. Charge carrier hopping transport based on marcus theory and variable-range hopping theory in organic semiconductors. *Journal of Applied Physics*, 118(4):045701, 2015.
- [148] I. I. Fishchuk, A. Kadašchuk, S. T. Hoffmann, S. Athanasopoulos, J. Genoe, H. Bässler, and A. Köhler. Unified description for hopping transport in organic semiconductors including both energetic disorder and polaronic contributions. *Phys. Rev. B*, 88:125202, Sep 2013.
- [149] Zhigang Shuai, Weitang Li, Jiajun Ren, Yuqian Jiang, and Hua Geng. Applying marcus theory to describe the carrier transports in organic semiconductors: Limitations and beyond. *The Journal of Chemical Physics*, 153(8):080902, 2020.
- [150] Guangjun Nan, Linjun Wang, Xiaodi Yang, Zhigang Shuai, and Yi Zhao. Charge transfer rates in organic semiconductors beyond first-order perturbation: From weak to strong coupling regimes. *The Journal of Chemical Physics*, 130(2):024704, 2009.